universität wien

MASTERARBEIT / MASTER'S THESIS

Titel der Masterarbeit / Title of the Master's Thesis

„AMPK and NRF2: Insights into the molecular interplay between two cell stress regulators“

verfasst von / submitted by

Sylvia Ender, BA BSc

angestrebter akademischer Grad / in partial fulfilment of the requirements for the degree of

Magistra pharmaciae (Mag.pharm.)

Wien, 2023 / Vienna 2023

Studienkennzahl lt. Studienblatt / degree programme code as it appears on the student record sheet:	UA 066 605
Studienrichtung lt. Studienblatt / degree programme as it appears on the student record sheet:	Masterstudium Pharmazie
Betreut von / Supervisor:	Assoz. Prof. Dipl.-Biochem. Dr. Elke Heiß
Mitbetreut von / Co-Supervisor:	Eleni Petsouki, PhD

Abstract

The transcription factor NRF2 and the serine/threonine kinase AMPK regulate the cellular response to redox and energy stress, respectively. Due to their concomitant activation when exposed to certain natural products and the overlapping cellular processes induced by NRF2 and AMPK signaling, a certain cooperativity between NRF2 and AMPK has been reported in previous studies. Recently, our lab has discovered three targets of AMPK-dependent phosphorylation (Ser374, 408, 433), which are located within or near to the Neh6 domain that is responsible for the β-TrCP-mediated ubiquitination of NRF2.

The aim of this thesis was to examine how the identified AMPK-dependent phospho-sites on NRF2 can affect its β-TrCP2-mediated degradation. Therefore, the wild type form of NRF2 (WT-NRF2) was compared with triple mutant (TM-)NRF2 (mutation of Ser374, 408,433 to Ala) in terms of their protein half-life, their interaction with β-TrCP2 and their expression of the NRF2 target gene *Gclc*. In order to unmask the effects of β-TrCP2 in the degradation of NRF2, the respective half-life experiments, proximity ligation assays and qPCR assays were performed using KEAP1 depleted MEF cells. KEAP1 inactivation results in NRF2 hyperactivation and has been involved in many pathological conditions including cancer. Experiments were further conducted with and without the presence of the AMPK-activator A-769662 to investigate the influence of AMPK in more detail.

The data showed that mutation of the AMPK-dependent phosphorylation sites in NRF2 caused an increase in NRF2 protein stability. This is likely the consequence of the impeded interaction between TM-NRF2 and β-TrCP2 as was revealed using PLA. In addition, upon exposure to the AMPK-activator A-769662, PLA results demonstrated an enhanced nuclear interaction of NRF2 forms with β-TrCP2. Furthermore, mutation of the phosphorylation sites seems to also affect NRF2 target gene expression, as qPCR results show that TM-NRF2 elicits higher *Gclc* expression than WT-NRF2.

Overall, the data suggest that the AMPK-dependent phosphorylation at the three serine residues in NRF2 promotes its interaction with β-TrCP2, thus facilitating its degradation in a β-TrCP2-dependent manner and leading to a decrease in the expression of selected NRF2 target genes.

Zusammenfassung

Der Transkriptionsfaktor NRF2 reguliert die zelluläre Reaktion auf oxidativen Stress – die Serin/Threonin Kinase AMPK die Reaktion auf Stress bedingt durch Energiemangel. Da bestimmte Naturstoffe beide Zellstressregulatoren zugleich aktivieren und die von NRF2 und AMPK hervorgerufenen Zellprozesse sich teilweise überlappen, wurde in der Forschung schon länger ein gewisses Zusammenspiel zwischen NRF2 und AMPK angenommen. Tatsächlich hat unsere Arbeitsgruppe kürzlich die AMPK-abhängige Phosphorylierung von NRF2 an drei Serinresten (Ser374, 408, 433) festgestellt, die sich in oder nahe der Neh6 Domäne befinden, welche für die Ubiquitinierung von NRF2 durch β-TrCP2 verantwortlich ist.

Das Ziel der vorliegenden Arbeit war es zu untersuchen, wie die von AMPK abhängigen Phosphorylierungsreste auf NRF2 den durch β-TrCP2 gesteuerten Abbau von NRF2 beeinflussen. Aus diesem Grund wurde Wildtyp-NRF2 (WT-NRF2) mit triple mutant (TM-)NRF2 (Ser374, 408, 433 mutiert zu Ala) in Bezug auf Halbwertszeit, Interaktion mit β-TrCP2 und Expression des für NRF2 spezifischen Gens *Gclc* verglichen. Um den Effekt von β-TrCP2 auf den Abbau von NRF2 zu erkennen, wurden die jeweiligen Experimente zu Halbwertszeit, Proximity Ligation Assay und qPCR unter Benutzung von KEAP1-defizienten MEF-Zellen durchgeführt. Inaktivierung von KEAP1 führt zu einer verstärkten Aktivierung von NRF2 und spielt in einer Reihe von pathologischen Zuständen, unter anderem Krebs, eine Rolle. Die Experimente fanden sowohl mit als auch ohne den AMPK-Aktivator A-769662 statt, um den Effekt von AMPK besser beurteilen zu können.

Die Ergebnisse zeigten, dass die Mutation der von AMPK phosphorylierten Serinreste die Proteinstabilität von NRF2 erhöht. Das ist wahrscheinlich durch die herabgesetzte Interaktion zwischen TM-NRF2 und β-TrCP2 zu erklären, die mittels PLA beobachtet werden konnte. Zudem ist anhand der PLA-Ergebnisse eine gesteigerte Interaktion zwischen NRF2 und β-TrCP2 im Nukleus nach Zugabe des AMPK-Aktivators A-769662 erkennbar. Außerdem wirkt sich die Mutation der Phosphorylierungsstellen auch auf die Expression der für NRF2 spezifischen Gene aus, da die qPCR-Ergebnisse eine höhere *Gclc*-Genexpression bei TM-NRF2 im Vergleich zu WT-NRF2 aufweisen.

Generell führen die Ergebnisse dieser Arbeit zu der Annahme, dass die AMPK-abhängige Phosphorylierung an den drei Serinresten die Interaktion von NRF2 mit β-TrCP2 erhöht. Dadurch wird der von β-TrCP2 abhängige Abbau von NRF2 gesteigert, was infolgedessen die von NRF2 kontrollierte Genexpression erniedrigt.

Table of Contents

1 Introduction

In everyday life the human body is constantly exposed to various external stimuli, like UV light, diesel exhaust or industrial toxins, that trigger the production of reactive oxygen species (ROS). In addition, many physiological cellular processes generate ROS as a byproduct. High levels of ROS within the cells lead to oxidative stress which ultimately causes oxidative damage to cellular lipids, proteins, and nucleic acids. To protect themselves against oxidative stress, cells rely on a complex antioxidant defense system, a master regulator of which is the nuclear factor erythroid 2-related factor (NRF2) [1].

NRF2 regulates cellular redox homeostasis and thus plays an important role in cytoprotection. However, constitutively elevated NRF2 activity has been linked to tumor progression in some cancer types [2,3] such as non-small cell lung cancer (NSCLC) [4–6]. In many of these cases, aberrant upregulation of NRF2 is caused by the inactivation of the Kelch-like ECH-associated protein 1 (KEAP1), the major negative regulator of NRF2, through somatic mutations or epigenetic modifications. This leads to an increased NRF2-induced transcription of antioxidative cytoprotective genes that protect the tumor cells and can induce resistance to chemotherapeutic drugs and other cancer treatments [2–6]. Hence, a better understanding of the KEAP1-independent regulation of NRF2 is highly relevant and will help to advance the research into the treatment of cancers with hyperactive NRF2.

In this regard, the attention of our lab has recently focused on the 5′-AMP-activated protein kinase (AMPK) and its interplay with NRF2 [7–9]. AMPK acts as a major nutrient and energy sensor and is crucial for maintaining cellular energy homeostasis. Taken together, AMPK and NRF2 function as major cellular stress sensors responsible for upholding energy and redox balance, respectively. In view of this, it has become apparent that both stress sensors are activated concomitantly by certain compounds and induce overlapping cellular responses [10]. Therefore, the potential molecular crosstalk between AMPK and NRF2 has become a topic of current research.

This master thesis investigates the interplay of AMPK and NRF2 specifically under KEAP1-depleted conditions as they occur in certain cancer cells. More precisely, the main objective was to examine how the phosphorylation of NRF2 by AMPK impacts the regulation of NRF2 by a less prominent regulator of NRF2 – that is the β-transducing repeat-containing protein (β-TrCP).

1.1 Nuclear factor erythroid 2-related factor 2 (NRF2)

NRF2 is a ubiquitously expressed transcription factor and a major regulator of the cellular antioxidant defense, further it is also involved in cell proliferation, lipid metabolism, detoxification and drug metabolism [11]. In this role NRF2 targets over 250 genes [12–14], such as heme oxygenase 1 (*Hmox1*), an enzyme essential for iron metabolism and oxidative stress response [15], NAD(P)H quinone dehydrogenase 1 (*Nqo1*), which is playing a prominent role in xenobiotic detoxification and redox balance [16] and glutamate-cysteine ligase catalytic subunit (*Gclc*), one of the proteins involved in controlling glutathione synthesis [17]. While NRF2 usually initiates the expression of its targets, it can also downregulate certain genes – one of which is Dual specificity phosphatase 4 (*DUSP4*) [18].

The transcription factor NRF2 belongs to the family of the cap´n´collar (CNC) basic region leucine zippers (bZIP) [19]. The number of amino acids and its molecular weight slightly vary as several different human NRF2 isoforms have been reported. Though, most frequently mentioned for NRF2 are a length of 605 amino acids and a mass of approximately 68 kDa [20]. As for the structure of NRF2, it consists of seven NRF2-ECH homology (Neh) domains of which each has its own distinct function (Fig. 1). Neh1 is the CNC-bZIP region and thus serves as the DNA-binding region [19]. The Neh2 domain negatively regulates NRF2 as it is the binding-site for KEAP1 leading to ubiquitination and proteasomal degradation of the transcription factor [21]. The regions Neh3-5 are transactivation domains that promote the transcription of target genes [22,23]. Neh6 has a negative impact on NRF2 stability by recruiting β-TrCP [24]. Lastly, domain Neh7 associates with the retinoid X receptor α (RXRα) in the nucleus resulting in reduced transcriptional activity of NRF2 [25].

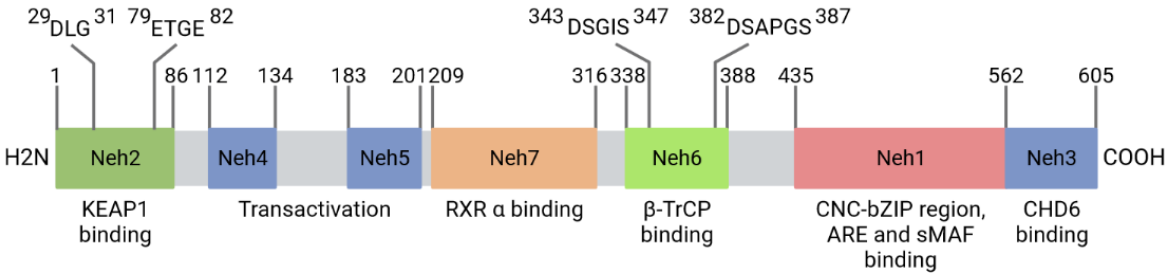

Figure 1 **Domain structure of NRF2**

The conserved Neh domains and their positions within the human NRF2 isoform consisting of 605 amino acids are depicted. The positions of the KEAP1-binding motifs (DLG[31] and ETGE[82]) and the β-TrCP-binding motifs (DSGIS[347] and DSAPGS[387]) are shown. The main function of each Neh domain is illustrated. Figure created with BioRender.com.

1.1.1 Activation of NRF2 during oxidative stress

Under homeostatic conditions, basal NRF2 levels remain low due to its high turnover mediated by KEAP1. Upon exposure to oxidative stress or certain compounds [26] KEAP1-dependent degradation of NRF2 decreases, thus enhancing NRF2 stability and nuclear translocation (Fig. 3) [26–28]. Once in the nucleus, the Neh1 domain of NRF2 dimerizes with small musculoaponeurotic fibrosarcoma (sMAF) proteins and then binds to the antioxidant response element (ARE), a DNA sequence located in the promoter region of NRF2 target genes [29]. Subsequently, NRF2 interacts with co-activators such as the CREB-binding protein (CBP), which binds to NRF2 via the Neh4 and Neh5 domains [22], or the chromodomain helicase DNA-binding protein 6 (CHD6) interacting with Neh3 [23]. Finally, together with its co-activators NRF2 recruits a mediator complex [30], which transmits the activation signal from the transcription factor to the RNA polymerase II [31].

1.1.2 Regulation of NRF2

NRF2 activity is regulated extensively and on multiple levels. However, the strongest impact on the general activation of NRF2 has its cellular abundance, which is mainly determined by the protein´s degradation [11,31]. Responsible for proteasomal degradation of NRF2 is above all KEAP1 and to a lesser extent also β-TrCP [32].

1.1.3 Kelch-like ECH-associated protein 1 (KEAP1)

KEAP1 is a substrate adaptor protein for the Cullin-3 (CUL3)/RING box protein 1 (RBX1) E3 ubiquitin ligase causing the conjugation of ubiquitin to its substrates [33]. Existing in the cell as a homodimer [34], its subunits consist of three functional domains (Fig. 2A): the BTB dimerization domain [21], the central intervening region (IVR) with several cysteine residues acting as redox sensors [35] and the Kelch repeat domain responsible for substrate capture [21].

As for the interaction with NRF2, a shallow pocket located within the Kelch domain of KEAP1 serves as a binding site for the Neh2 region of NRF2 [36]. Neh2 contains two KEAP1-binding motifs, the low-affinity DLG^{31} and the high-affinity $ETGE^{82}$ motif [37,38]. During KEAP1-NRF2 association these motifs each bind to one of the two Kelch regions of the KEAP1 dimer, thus stabilizing the lysine residues located between them (Fig. 2B) [34]. Each KEAP1 molecule connects to CUL3 of the CUL3/RBX1 E3 ubiquitin ligase complex via the BTB and IVR regions (Fig. 2) [33,39]. Thus, through KEAP1 the E3 ubiquitin ligase complex can access its target, allowing the final stage of the ubiquitination process to happen [overview in Buetow and Huang 2016, 40]. In this step the E3 ubiquitin ligase binds the E2 ubiquitin conjugating enzyme and thus catalyzes the binding of ubiquitin to certain lysine residues, which for NRF2 are located between the ETGE and DLG motifs immobilized by KEAP1 [37]. The poly-ubiquitinated NRF2 is then targeted for proteasomal degradation (Fig. 3A) [41].

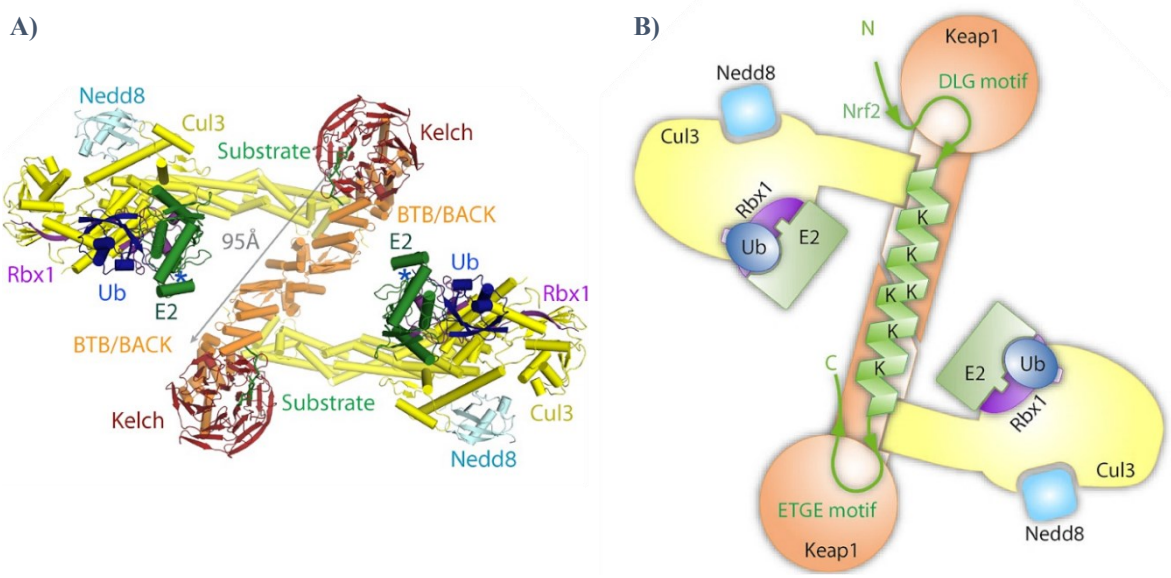

Figure 2 **Model of the fully assembled KEAP1/CUL3/RBX1 E3 ubiquitin ligase complex**

(A) Structural model of a BTB-Kelch/CUL3/RBX1 E3 ubiquitin ligase complex. (B) Schematic illustration of NRF2 recruitment by the KEAP1/CUL3/RBX1 E3 complex in accordance with the structural model proposed in (A). Binding of the DLG[31] and ETGE[82] motifs to the Kelch regions of the KEAP1 dimer effectively fixates the intervening α-helix containing the lysine residues targeted for ubiquitination by the CUL3/RBX1 E3 complex. Figure reused from Canning et al. 2013 [39], licensed under Creative Commons Attribution (CC BY 4.0).

NRF2 activation through inhibiting KEAP1 function is usually caused by the binding of electrophilic molecules to specific cysteines in the IVR region of KEAP1 [26]. This does not disrupt the binding of Neh2 to KEAP1 though, meaning that oxidative stress does not lead to the dissociation of NRF2. Hence, as an explanation for rising cellular NRF2 levels after the exposure of KEAP1 to electrophilic stimuli the "Hinge & Latch" model has been proposed [42]. This model is based on the difference between the ETGE and DLG motifs concerning binding kinetics and affinity to KEAP1, more precisely the slow association and dissociation but high affinity binding of the ETGE motif and the fast but weak interactions of DLG [38]. The hypothesis is as follows: The interactions of electrophiles with the cysteine residues of the IVR domain induce a conformational change in KEAP1, that has no impact on the binding of ETGE, but diminishes association with DLG. Thus, KEAP1 cannot properly fixate the Neh2 domain anymore and therefore not facilitate the ubiquitination of NRF2. Still, it binds NRF2 with high affinity via ETGE and as a result is blocked from interacting with further substrates. This implies that the accumulation of NRF2 after KEAP1 inactivation is due to *de novo* synthesized protein, which is no longer targeted for ubiquitination (Fig. 3B) [20,36,43].

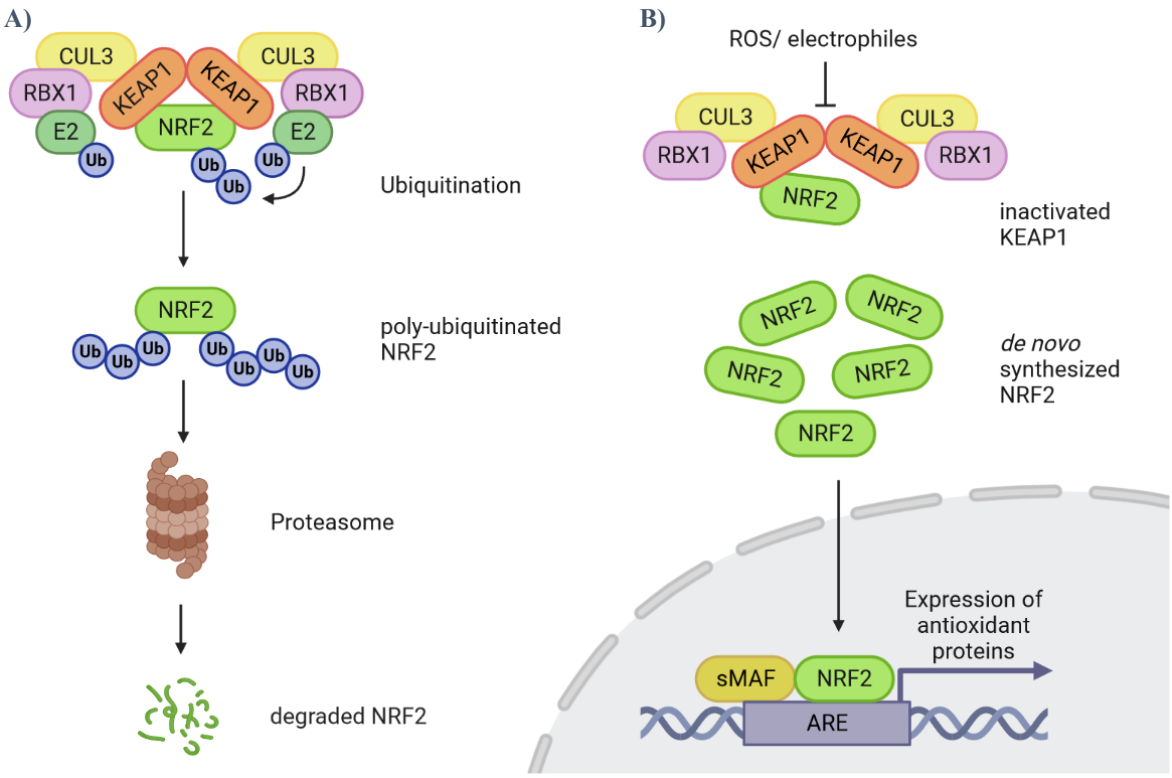

Figure 3 **NRF2/KEAP1 pathway**
(A) Under homeostatic conditions cellular NRF2 levels remain low due to high proteasomal degradation mediated by the KEAP1/CUL3/RBX1 E3 ubiquitin ligase complex. (B) Under oxidative stress KEAP1-NRF2 interaction ceases to exist allowing NRF2 to translocate into the nucleus and activate its target genes. Figure created with BioRender.com.

1.1.4 β-transducing repeat-containing protein (β-TrCP)

The second major degradation pathway of NRF2 is controlled by β-TrCP, another adaptor protein for a E3 ubiquitin ligase complex. The ligase is known as the S-phase kinase-associated protein 1 (SKP1)-Cullin-1 (CUL1)-F-box (SCF) E3 ubiquitin ligase and β-TrCP serves as one of its F-box proteins. These proteins are responsible for substrate recognition and binding and are divided in sub classes according to their substrate binding motifs. β-TrCP belongs to the F-box and WD repeat domain containing (FBXW) class and exists as the isoforms FBXW1 and 11, or β-TrCP1 and β-TrCP2 respectively [44,45]. Both β-TrCP isoforms seem to be involved in NRF2 regulation [24]. Structurally, three functional domains of β-TrCP are known: The D domain for dimerization, the F-box domain necessary for binding to SKP1 of the E3 ubiquitin ligase complex and seven WD40 repeats, which enable recognition and binding of substrates (Fig. 4A) [46]. The β-TrCP isoforms may exist as dimers in the cell and while homodimerization seems to promote the ligase activity of the $SCF^{\beta\text{-}TrCP}$ complex, β-TrCP1/β-TrCP2 heterodimerization mediates self-degradation of the F-box proteins [45,46].

NRF2 interacts with β-TrCP via its Neh6 domain, which harbors two distinct recognition motifs necessary for β-TrCP-binding: $DSGIS^{347}$ and $DSAPGS^{387}$ (Fig. 4A) [47]. In the case of β-TrCP, binding one of these two recognition motifs of NRF2 is sufficient to activate its ubiquitylation. Further, it has been shown that phosphorylation of Ser344 and/ or Ser347 within DSGIS by the glycogen synthase kinase-3 (GSK-3) enhances interactions between NRF2 and β-TrCP [24,47–49]. However, while GSK-3 increases ubiquitylation via the DSGIS motif by creating a phosphodegron for β-TrCP, the kinase has no influence on the degradation through DSAPGS. Thus, GSK-3 activity is not essential for ubiquitylation of NRF2, but enhances it (Fig. 4B) [47]. After association of the $SCF^{\beta\text{-}TrCP}$ complex with its substrate NRF2 the E3 ubiquitin ligase facilitates the transfer of ubiquitin from the E2 conjugating enzyme [overview in Bi et al. 2021, 46], subsequently leading to the proteasomal degradation of NRF2 (Fig. 4).

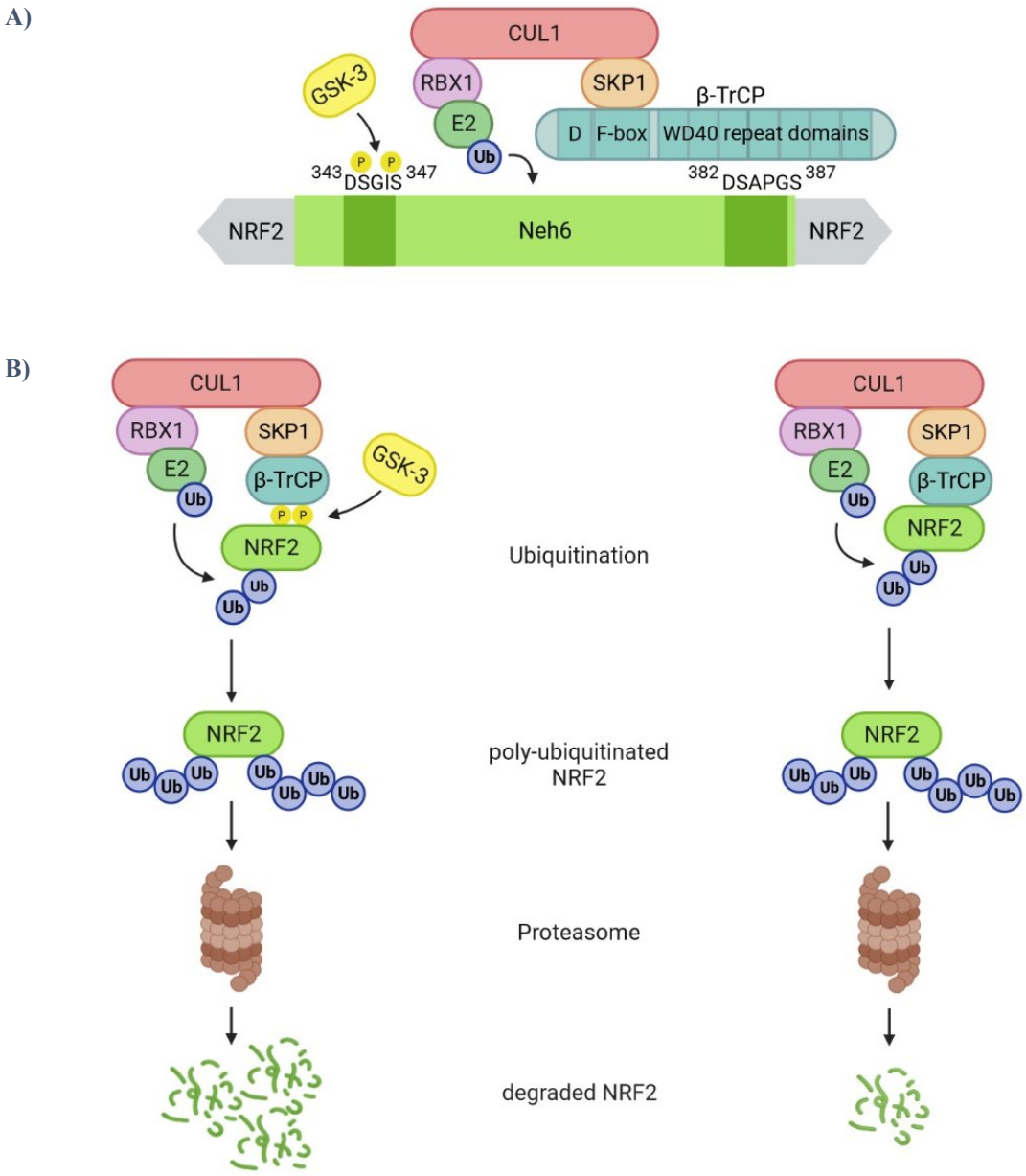

Figure 4 **β-TrCP-mediated degradation of NRF2**

(A) Schematic illustration of NRF2 recognition by the $SCF^{β\text{-}TrCP}$ E3 ubiquitin ligase complex via the $DSAPGS^{387}$ motif in Neh6. The WD40 repeat domains of β-TrCP interact with the $DSGIS^{347}$ or the $DSAPGS^{387}$ recognition motif of NRF2 and the F-box domain binds to SKP1 of the E3 ubiquitin ligase. The D domain regulates homo- or heterodimerization of β-TrCP. (B) NRF2 degradation by β-TrCP occurs in the presence as well as absence of GSK-3. GSK-3 phosphorylation of Ser344 and/ or Ser347 as depicted in (A) enhances β-TrCP-mediated NRF2 degradation. Figure created with BioRender.com.

1.1.5 Contribution of KEAP1 and β-TrCP to NRF2 regulation

To begin with, the subcellular localization of KEAP1 and β-TrCP may have an impact on their role in regulating NRF2 levels [47]. KEAP1 is known to primarily exist in the cytoplasm [50], whereas both isoforms of β-TrCP are localized in the cytoplasm as well as the nucleus [51]. Further, the KEAP1 and β-TrCP degradation pathways are controlled through different mechanisms [52]. While the KEAP1/ NRF2 system operates according to the cells oxidative stress, ubiquitination of NRF2 via β-TrCP can be affected by GSK-3 activity. GSK-3 phosphorylates its targets predominantly under resting conditions and has its enzymatic activity reduced through extracellular signals like growth factors and hormones [32,49]. Overall, due to massively down-regulating NRF2 under basic conditions, KEAP1 is considered to be the "limiter valve" of NRF2 abundance. β-TrCP on the other hand serves as a "regulator valve" adjusting the NRF2 levels to current metabolic demands [49]. Recent research on the cooperation of KEAP1 and β-TrCP pathways in mice indicates that in the case of severely suppressed KEAP1function β-TrCP may act as a safeguard system managing to keep NRF2 at non-pathological levels [52]. However, it seems unclear if in the case of severe KEAP1 suppression β-TrCP actually assumes a more prominent role in NRF2 repression or if the effects of β-TrCP are simply unmasked and better visible.

1.2 5´-AMP-activated protein kinase (AMPK)

AMPK is a ubiquitously occurring heterotrimeric serine/threonine kinase and acts as a major regulator of cellular energy metabolism. Its activation is usually the result of elevated AMP : ATP ratios and high calcium levels as well as a reduction in glucose supply. Once activated, AMPK drives the cell´s metabolism towards catabolism by promoting glucose uptake, glycolysis, fatty acid oxidation, autophagy and mitophagy. Anabolic processes on the other hand like glycogen synthesis, gluconeogenesis, fatty acid and cholesterol synthesis as well as protein and RNA syntheses are downregulated [recent reviews on AMPK in 53–56]. Further, AMPK also indirectly responds to redox changes in the cell and plays a role in antioxidant defense [57,58].

Concerning overall structure, AMPK consists of the catalytic α-subunit and the regulatory β- and γ-subunits, each existing as multiple isoforms thus allowing for a number of tissue-specific combinations [59]. The α-subunit contains a conventional kinase domain (α-KD) followed by an auto-inhibitory domain (α-AID) which induces a less active conformation in the α-KD, further an α-linker and a carboxy-terminal domain (α-CTD). As for the β-subunit, it includes a carbohydrate binding module (β-CBM) and a carboxy-terminal domain (β-CTD), which is necessary for interacting with the α-CTD and the γ-subunit and is thus vital for forming the stable core of the AMPK complex. The γ-subunits harbor four tandem repeats named cystathionine β-synthase (CBS1-4) motifs. These regions serve as the AMP/ADP/ATP binding sites (Fig. 5) [AMPK structure reviewed in 56,60].

1.2.1 Activation of AMPK

The activity of AMPK is controlled by multiple compounds and enzymes interacting with several sites in the AMPK complex. Only the most prominent of these regulators shall be briefly discussed here. Essential for the activation of AMPK is the phosphorylation of a conserved threonine residue (Thr172) within the activation loop of the carboxy-terminal lobe (C-lobe) of the α-KD as this stabilizes and adjusts the position of the aforementioned activation loop [61]. Threonine 172 is the phosphorylation target of the liver kinase B1 (LKB1) and the calcium/calmodulin-dependent protein kinase kinase 2 (CAMKK2) – hence these enzymes act as upstream kinases of AMPK and are crucial for AMPK activation [62,63].

Adenine nucleotides bind with varying affinity to the CBS1, 3 and 4 regions of the γ-subunit [64]. Upon AMP-binding to CBS3 – the binding site with the highest affinity for adenine nucleotides, CBS3 interacts with the regulatory subunit-interacting motif 2 (α-RIM2) located in the α-linker domain thus initiating a conformational change in the α-subunit that shifts the inhibitory α-AID away from the kinase domain [54,65] and protects the phosphorylated Thr172 residue by pulling the catalytic and nucleotide-binding modules together [54,66,67]. Moreover, AMP-binding has also been reported to induce contacts between the γ-subunit and the activation loop. These interactions promote the stabilization of the activation loop as well as the protection of Thr172 against dephosphorylation [61]. In summary, AMP functions as an allosteric regulator of AMPK and on a more important note also prevents dephosphorylation of Thr172.

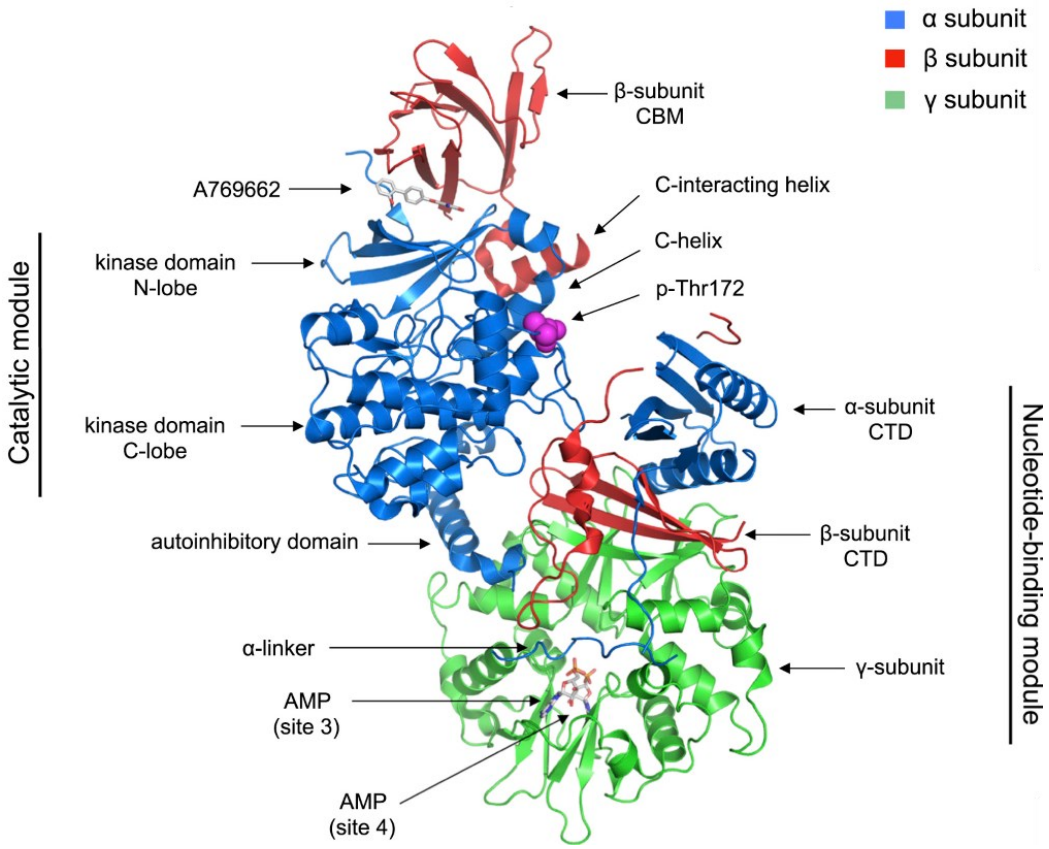

Figure 5 **Backbone structure of the AMPK complex**
The crystal structure of the backbone of the AMPKα2β1γ1 complex and its major structural domains are illustrated. AMPK is shown in its active form with phosphorylated Thr172 and two AMP molecules bound to the CBS sites 3 and 4, respectively. Structural conformation indicates interactions between the α-linker and the AMP-bound γ-subunit. The AMPK activator A-769662 is depicted within the ADaM-site, a pocket formed between the β-CBM and the α-KD. Figure adapted from Garcia and Shaw 2017 [55], with permission from Elsevier.

1.2.2 A-769662

The A-769662 compound functions as a direct activator of AMPK. Similar to AMP it also increases AMPK activity allosterically and inhibits Thr172 dephosphorylation [68]. It has a different interaction site though, as it binds into a pocket formed between the β-CBM and the α-KD known as the allosteric drug and metabolite (ADaM)-binding site [56]. Crucial for the activation of AMPK by A-769662 is the phosphorylation of Ser108 within the β-subunit, presumably because it is necessary for the stability of the ADaM site [61,69]. Upon occupying its binding pocket, A-769662 appears to promote the interaction between the activation loop and the regulatory γ-subunit thus impeding the dephosphorylation of Thr172 and allowing the activation loop to become ordered [70]. Moreover, by stabilizing the activation loop in the kinase domain A-769662 is even able to moderately activate AMPK independently of Thr172 phosphorylation [69,70].

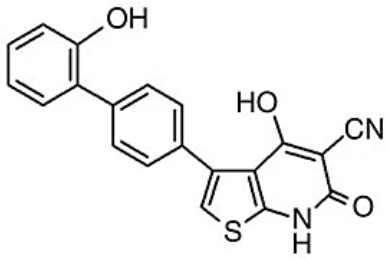

Figure 6 **Chemical structure of A-769662**

1.2.3 Some prominent targets of AMPK

Activated AMPK shapes cellular energy metabolism via the phosphorylation of certain Ser/Thr residues within its numerous downstream targets [AMPK recognition motif reviewed in 54]. Some of the more prominent substrates of AMPK shall be mentioned here.

Concerning glucose metabolism AMPK´s role includes the phosphorylation of TBC1 domain family member 1 and 4 (TBC1D1/4) which initiates the translocation of the glucose transporter type 4 (GLUT4) to the cell surface and thus increases glucose uptake into the cell [71]. Regarding the cell´s lipid metabolism AMPK for instance upregulates fatty acid oxidation via inhibiting the acetyl-CoA carboxylase 2 (ACC2) and impedes fatty acid synthesis via the acetyl-CoA carboxylase 1 (ACC1) as well as cholesterol synthesis via the 3-hydroxy-3-methyl-glutaryl-CoA reductase (HMGCR) [AMPK´s effect on lipid metabolism reviewed in 72]. Further, AMPK promotes autophagy via activating the unc51-like autophagy activating kinase 1 (ULK1) and negatively regulating the mechanistic target of rapamycin complex 1 (mTORC1) [AMPK on autophagy recently reviewed in 73]. This impeding effect on mTORC1 is conveyed through the phosphorylation of the tuberous sclerosis complex 2 (TSC2) and the regulatory-associated protein of mTOR (RPTOR) and additionally leads to a reduction in protein synthesis [AMPK and mTOR recently reviewed in 74].

Another aspect of the cell´s metabolism affected by AMPK is mitochondrial homeostasis. AMPK stimulates mitochondrial biogenesis via activating the peroxisome proliferator-activated receptor gamma co-activator 1α (PGC1α), which is a co-activator enhancing the transcription of mitochondrial genes. Also, AMPK-dependent activation of ULK1 promotes mitophagy, a process necessary for maintaining mitochondrial integrity [AMPK on mitochondrial homeostasis reviewed in 75].

Overall, activation of AMPK affects many cellular pathways with the aim of restoring energy homeostasis by promoting catabolic processes that increase ATP synthesis and repressing anabolic ATP-consuming processes [AMPK phosphorylation targets reviewed in detail in 55].

1.3 AMPK and NRF2 signaling – Overlapping cellular response

Both NRF2 and AMPK act as stress sensors regarding cellular defense and energy metabolism, respectively – they also show a certain overlap in the processes they affect in the cell. As an example, phosphorylation by AMPK activates enzymes involved in fatty acid oxidation and inhibits those in charge of fatty acid synthesis. NRF2 has a comparable effect on the lipid metabolism by upregulating the transcription of genes encoding enzymes needed for fatty acid oxidation and negatively regulating transcription of those responsible for lipid biosynthesis [11]. Furthermore, NRF2 is also involved in autophagy. While AMPK upregulates autophagy in general by increasing activity of ULK1, NRF2 upregulates the transcription of Sequestosome 1 (SQSTM1), a cargo receptor that selectively binds proteins for autophagy. Incidentally, upregulation of SQSTM1 creates a positive feedback loop for NRF2 since it targets KEAP1 and thus impedes NRF2 degradation [76]. Same as AMPK, NRF2 is also heavily involved in mitochondrial homeostasis. NRF2 influences mitochondrial biogenesis by upregulating the transcription of the alpha palindromic-binding protein (alpha-PAL) and the mitochondrial transcription factor A (TFAM), which in turn function as transcription factors responsible for the expression of mitochondrial genes. In addition, NRF2 is also involved in mitophagy by increasing expression of the phosphatase and tensin homolog (PTEN)-induced kinase 1 (PINK1), which recognizes damaged mitochondria, and by upregulating the autophagic cargo protein SQSTM1. Apart from that, NRF2 is crucial for preserving mitochondrial redox homeostasis as the respiration process is the primary source of endogenous ROS production [77,78]. As a last common feature of AMPK and NRF2 signaling to be addressed here, AMPK activation to a certain extent helps alleviating redox stress. This is due to its inhibition of fatty acid synthesis and promotion of fatty acid oxidation, which indirectly increases the generation of NADPH – a cofactor required in many antioxidant pathways [79].

1.4 AMPK and NRF2 signaling – Natural products

Interdependence between AMPK and NRF2 signaling is further substantiated by the antioxidative properties of many natural products that have been shown to simultaneously influence both AMPK and NRF2. A review about recent research on natural products affecting AMPK and NRF2 signaling was conducted by Petsouki et al. 2022, which also includes references regarding the model system, the identified signaling axis and the tested pathophysiological relevance of each researched compound [10]. In many cases, examination of the cellular effects of these natural compounds led to establishing involvement of an AMPK/NRF2 signaling axis, without further investigating the exact mechanisms of the discovered crosstalk. This applies as an example for the research done on berberine [80], maackiain [81], aucubin [82] or resveratrol [83,84]. Besides that, some reports specify that their respective natural products cause an increase in NRF2 activity via the AMPK-dependent inhibitory phosphorylation of GSK-3β (see Ch. 1.5). This is the case for instance with betulin [85], xanthohumol [86], butin [87], corilagin [88] and pterostilbene [89]. Another prominent natural compound, sulforaphane – primarily known for targeting the KEAP1/NRF2 pathway, has recently also been suggested to affect NRF2 via AMPK/GSK-3β signaling [90]. Nevertheless, in many cases the precise effect of the phytochemicals on AMPK and/or NRF2 signaling remains elusive, thus making it all the more important to investigate the crosstalk between AMPK and NRF2 in more detail.

1.5 Crosstalk between AMPK and NRF2

Due to the many natural products affecting both AMPK and NRF2, as well as the overlap in cellular response to AMPK and NRF2 signaling, a certain interplay between the two stress sensors is to be expected. In this regard, downstream effects of AMPK have been shown to influence NRF2 regarding many aspects such as protein stability or transactivation capability.

1.5.1 Indirect interaction between AMPK and NRF2

To start, AMPK is involved in the SQSTM1-mediated degradation of KEAP1. On one hand, AMPK acts as one of the protein kinases that directly phosphorylate SQSTM1 at Ser351, which increases the binding of SQSTM1 to KEAP1 and therefore its degradation [91]. On the other hand, SQSTM1 facilitates increased interaction between AMPK and ULK1, which induces autophagy thus further boosting the depletion of KEAP1 [92]. This effect of AMPK on KEAP1 reduces degradation of NRF2. Besides that, AMPK also influences NRF2 degradation via the GSK-3/β-TrCP axis since AMPK has been reported to inhibit GSK-3β [93]. Thus, the GSK-3 facilitated interaction between β-TrCP and NRF2 as mentioned above (Ch. 1.1.4) is impeded by AMPK activation and therefore NRF2 is upregulated. Another mechanism of AMPK exercising influence on NRF2 is via repressing the BTB domain and CNC homology 1 (BACH1) transcription regulator protein. BACH1 acts as a competitor to NRF2 as it also binds to the ARE sites, but mainly downregulates the expression of ARE-regulated genes [94]. AMPK activity has been shown to reduce BACH1 abundance leading to an enhanced transactivation of selected ARE-regulated genes due to the changed NRF2 : BACH1 ratio [8].

1.5.2 NRF2 – A phosphorylation target of AMPK

Apart from AMPK´s downstream signaling having an impact on NRF2, recent findings reported that NRF2 is also a direct target of AMPK-mediated phosphorylation. The first AMPK-mediated phosphorylation site discovered in NRF2 was the serine residue 558, which in its phosphorylated form prevents the nuclear export of NRF2 causing its accumulation in the nucleus [93]. Besides that, Matzinger et al. 2020 discovered Ser374, Ser408 and Ser433 of NRF2 to be hyperphosphorylated upon AMPK activation. Following the detection of these phospho-sites, their function upon activation of AMPK with A-769662 was investigated in mouse embryonic fibroblasts (MEF) and human embryonic kidney cells (HEK293). In order to examine the role of the identified AMPK-dependent phospho-sites a triple mutant version of NRF2 (TM-NRF2) was created, which had Ser374, 408 and 433 replaced with alanine residues [7].

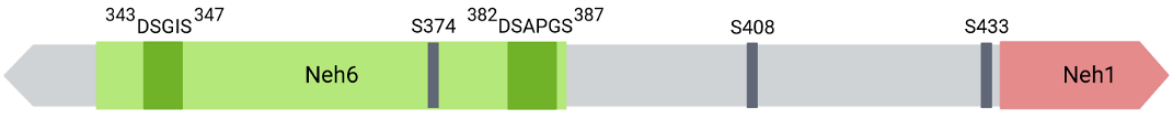

Figure 7 **Localization of the AMPK-dependent phosphorylation sites among the domains of NRF2**
The serine residues 374, 408 and 433, discovered as AMPK-dependent phosphorylation sites by Matzinger et al. 2020 [7], are illustrated in their relative positions within the NRF2 structure domain (see Fig. 1). They are located either within the Neh6 domain (Ser374) or in close proximity to the Neh6 and Neh1 domain (Ser408 and Ser433). Figure created with BioRender.com.

As the phospho-sites are located within or close to the Neh6 region (Fig. 7), which contains the β-TrCP recognition motifs, the contribution of the serine residues to the protein stability of NRF2 has been examined. However, no significant influence of the phospho-sites on the kinetics of NRF2 degradation could be detected in HEK or wild type MEF cells. In contrast, against a KEAP1 knockout background a difference in the stability of wild type (WT)- and TM-NRF2 was detected. The KEAP1-/- MEF cells expressing the mutated NRF2, which lacked the discovered AMPK-dependent phospho-sites, showed an extended NRF2 half-life in comparison to cells transfected with the wild type form of NRF2. Co-immunoprecipitation experiments using HEK cells co-expressing β-TrCP1 and WT- or TM-NRF2 demonstrated a generally reduced interaction between β-TrCP1 and TM-NRF2 when compared to the wild type, but also lessened β-TrCP1 interaction with WT-NRF2 upon AMPK activation. To explain these experimental results Matzinger et al. 2020 proposed the hypothesis that phosphorylation of the three serine residues renders WT-NRF2 a susceptible target for GSK-3 thus increasing its degradation via β-TrCP1. Upon AMPK activation GSK-3 was inhibited which explained the decreased interaction between WT-NRF2 and β-TrCP1 detected in the co-immunoprecipitation experiments. According to this model, replacement of the phosphorylation sites with alanine makes TM-NRF2 less receptive to GSK-3 phosphorylation, and thus impeded TM-NRF2 interaction with β-TrCP1 even without the influence of AMPK [7].

However, the proposed hypothesis contains one major discrepancy, that is the involvement of GSK-3. The experimental setup presented in the paper would render the GSK-3 mostly inactive due to its exposure to growth factors contained in the serum, which heavily downregulate the enzymatic activity of GSK-3 [32,49]. Therefore, it is debatable how much influence GSK-3 actually has on the presented results. Further research into the involvement of the AMPK-dependent phosphorylation sites in the regulation of NRF2 through β-TrCP remains necessary.

1.6 Aim of the thesis

The aim of this master thesis is to investigate how the AMPK-dependent phosphorylation of NRF2 at the three serine residues Ser374, Ser408 and Ser433 affects the regulation of NRF2 through β-TrCP in a KEAP1 depleted background. For this reason, NRF2/β-TrCP2 protein interaction, NRF2 stability and selected NRF2 target gene expression were examined in cells overexpressing β-TrCP2 alongside either wild type NRF2 (WT-NRF2) or a triple mutated version of NRF2, which had the three respective AMPK-dependent serine residues replaced with alanine (TM-NRF2). In order to better detect the impact of AMPK experiments were performed in the presence or absence of the AMPK activator A-769662. Further, all experiments were conducted using KEAP1-/- MEF cells. This approach was taken due to the strong repression of NRF2 by KEAP1, which masks the effects of β-TrCP on NRF2 [7]. Also, a KEAP1 depleted background is often observed in many pathological conditions including cancer [2–6], thus KEAP1-/- MEF cells may serve as a surrogate model for cancer cells with inactivated KEAP1.

2 Materials and Methods

2.1 Cell Culture

Technical Equipment

Name	Provider
HERAsafe™ KS 18 Workbench	Thermo Fisher Scientific Inc. (Waltham, MA, USA)
HERAcell™ 150 Incubator	Thermo Fisher Scientific Inc. (Waltham, MA, USA)
Heraeus™ Multifuge™ 1 S-R Centrifuge	Thermo Fisher Scientific Inc. (Waltham, MA, USA)
JULABO™ SW23 Shaking Water Bath	JULABO GmBH (Seelbach, Germany)
Olympus CKX41 Microscope	Olympus Optical Co. GmBH (Hamburg, Germany)
X-Cite™ 120Q Lumen Dynamics Fluorescence Lamp Illuminator	Excelitas Technologies Corp. (Waltham, MA, USA)
Vi-CELL™ XR Cell Viability Analyzer	Beckman Coulter (Brea, CA, USA)
VWR™ Analog Vortex Mixer	VWR International GmBH (Randor, PA, USA)
VWR™ Galaxy Mini Microcentrifuge	VWR International GmBH (Randor, PA, USA)
INTEGRA Pipetboy	INTEGRA Biosciences AG (Zizers, Switzerland)
Eppendorf Pipettes (0,5-10 µl, 2-20 µl, 10-100 µl, 100-1000 µl)	Eppendorf SE (Hamburg, Germany)

Consumables

Name	Provider
Serological Pipettes (5 ml, 10 ml, 25 ml)	Sarstedt AG & Co. KG (Nümbrecht, Germany)
Pipette tips (10 µl, 200 µl, 1000 µl)	Sarstedt AG & Co. KG (Nümbrecht, Germany)
Cell Culture Flask 75 cm2	Sarstedt AG & Co. KG (Nümbrecht, Germany)
Screw Cap Tubes (15 ml, 50 ml)	Sarstedt AG & Co. KG (Nümbrecht, Germany)
Cell Scraper	Greiner bio-one (Kremsmünster, Austria)
Cellstar™ 12 Well Cell Culture Plate	Greiner bio-one (Kremsmünster, Austria)
Cellstar™ 96 Well Cell Culture Plate	Greiner bio-one (Kremsmünster, Austria)
Eppendorf Safe-Lock Tubes 1,5 ml	Eppendorf SE (Hamburg, Germany)

Media, solutions and reagents

Name	Provider
Dulbecco´s Modified Eagle´s Medium (DMEM)	Sigma-Aldrich (St. Louis, MO, USA)
Fetal Bovine Serum (FBS) (S1810-500)	Biowest (Nuaillé, France)
BioWhittaker™ Penicillin/ Streptomycin mixture (Pen/ Strep) (DE17-602E)	Lonza Group (Basel, Switzerland)
L-Glutamine solution 200 mM (CAS-Nº. 56-85-9)	Sigma-Aldrich (St. Louis, MO, USA)
Trypsin 250X (CAS-Nº. 9002-07-7)	Gibco, via Thermo Fisher Scientific Inc. (Waltham, MA, USA)
Ethylenediamine tetraacetic acid (EDTA) disodium salt dihydrate ≥ 99 %, p.a., ACS (CAS-Nº. 6381-92-6)	Carl Roth (Karlsruhe, Germany)
Dimethyl sulfoxide (DMSO) ROTIPURAN® ≥ 99,8 %, p.a. (CAS-Nº. 67-68-5)	Carl Roth (Karlsruhe, Germany)
A-679662, 50 mg (CAS-Nº. 844499-71-4) (A3963)	APExBIO Technology (Houston, TX, USA)
Opti-MEM™ I Reduced Serum Medium	Gibco, via Thermo Fisher Scientific Inc. (Waltham, MA, USA)
Lipofectamine™ LTX and PLUS™ Reagent	Invitrogen, via Thermo Fisher Scientific Inc. (Waltham, MA, USA)

Name	Ingredients	
Growth Medium	DMEM	500 ml
	heat-inactivated FBS	10 %
	Glutamine	2 mM
	Penicillin/ streptomycin	1%
PBS	NaCl	36,0 g
	Na_2HPO_4	7,4 g
	KH_2PO_4	2,15 g
	H_2O dd	ad 5 000 ml
Trypsin/ EDTA in PBS	Trypsin	0,5 g
	EDTA	0,2 g
	PBS	ad 1 000 ml

Cell line

Name	Provider
KEAP1 -/- mouse embryonal fibroblasts (MEF)	kindly provided by Thomas Kensler (University of Pittsburgh, USA)

Plasmids

Name	Provider
EGFP-Myc-tagged WT-NRF2 (#21549)	Addgene (Watertown, MA, USA)
EGFP-Myc-tagged TM-NRF2	designed as previously described [7]
HA-tagged β-TrCP2 (#36969)	Addgene (Watertown, MA, USA)
Dharmacon™ ON-TARGETplus Mouse *FBXW11* (L-058886-00-0005) siRNA, 5 nmol (J-058886-05-0005)	Horizon Discovery Group (Cambridge, UK)
Dharmacon™ 5X siRNA Buffer (B-002000-UB-100)	Horizon Discovery Group (Cambridge, UK)
Dharmacon™ Molecular Grade RNase-free water (B-003000-WB-100)	Horizon Discovery Group (Cambridge, UK)

2.1.1 General Aspects

All procedures involving living cells took place under aseptic conditions and in a laminar air flow workbench. Solutions as growth media, PBS and Trypsin/ EDTA in PBS were prewarmed in a 37° C water bath before use as to not stress the cells at contact. When not used for experiments the cells were subcultured in 75 cm^2 Cell Culture Flasks and incubated at 37° C and 5 % CO_2.

2.1.2 Cell Passage

Passaging cells is crucial to ensure unstressed living conditions and growth for adherent cells such as MEF cells.

When cells became ~ 90 % confluent the old growth medium was removed, and cells were washed with 5 ml PBS. Then, in order to detach the cells from the surface of the flask, 2 ml of Trypsin/ EDTA was added. After 2-3 min incubation at 37° C and 5 % CO_2 trypsin was neutralized through adding 8 ml of growth medium. Cells were resuspended and transferred to a 50 ml Screw Cap Tube, then centrifuged at 210 x g for 5 min. The supernatant was removed, and the cells resuspended in 10 ml growth medium. At this step the concentration of resuspended cells could be analyzed with the Vi-CELL™ XR Cell Viability Analyzer. An aliquot with the required cell number was added to a new 75 cm^2 Cell Culture Flask with 15 ml of fresh growth medium.

Cells were passaged three times a week. After the 30^{th} passage cells were discarded, and new cells were thawed. Frozen cells were stored in 1 ml growth medium with 20 % serum and 10 % DMSO in liquid nitrogen. After defrosting, the cells were resuspended with 2 ml growth medium and added into a Screw Cap Tube with 8 ml growth medium, then centrifuged at 210 x g for 5 min. Afterwards the supernatant was removed and the cells resuspended in 1 ml growth medium, which was then added to a new 75 cm^2 Cell Culture Flask with 15 ml of fresh growth medium.

2.1.3 Transfection

In this thesis transfected cells overexpressing the examined proteins were used for experiments regarding Western-Blotting, Proximity Ligation Assay (PLA) and mRNA quantification.

In preparation for transfection the required number of cells were seeded in appropriate cell culture plates the day before (~ 60 000 cells/well for 12 Well Cell Culture Plates). Before starting the experiment, confluency of the cells, which should be at 70 to 90 %, was checked via microscopy. Then the required amount of Opti-MEM™ I Reduced Serum Medium, Lipofectamine™ LTX Reagent and PLUS™ Reagent as well as plasmids for each well was calculated in accordance with the Lipofectamine LTX® & PLUS™ Reagent Protocol 2013 by Invitrogen. Following the protocol, first Lipofectamine LTX reagent was diluted in Opti-MEM in an Eppendorf tube and incubated for 5 min at room temperature. Meanwhile plasmids and PLUS reagent were diluted in the same amount of Opti-MEM in a separate tube and later added to the aforementioned Eppendorf tube containing the Lipofectamine LTX reagent. The mix was incubated at room temperature for 15 min, then added to the appropriate wells (100 µl/well for 12 Well Cell Culture Plates).

Since the used plasmids for WT- and TM-NRF2 were EGFP- tagged, the success of the transfection of these plasmids could be analyzed under a fluorescence microscope the following day.

2.1.4 Transfection of siRNA

The transfection of siRNA was performed to knock down certain cellular proteins. Dharmacon™ reagents were used for siRNA transfection. During all steps of the transfection RNase-free filter tips and RNase-free tubes (see Ch. 2.5) were required as to not compromise the siRNA. Also, reagents and samples containing siRNA were not to be vortexed. Prior to transfection, a stock solution containing 20 µM of the desired siRNA was prepared. Therefore, the 5X siRNA Buffer was diluted 1:4 with RNase-free water and then 5 nmol of siRNA, viz. the entire purchased product, were added to 250 µl of the diluted siRNA-Buffer. The solution was then mixed via pipetting up and down, inverting ten times and finally putting it on a rotator for 30 min. Afterwards, transfection was performed as described above (Ch. 2.1.3) using the required amount of siRNA stock solution.

2.2 Amplification of plasmid DNA in bacteria

Technical Equipment

Name	Provider
MaxQ™ 4000 Benchtop Orbital Shaker	Thermo Fisher Scientific Inc. (Waltham, MA, USA)
B 15 Compact Incubator	Thermo Fisher Scientific Inc. (Waltham, MA, USA)
Sorvall® RC-5C Plus Superspeed Centrifuge	Kendro Laboratory Products (Newtown, CT, USA)
Heraeus™ Biofuge™ fresco Microcentrifuge	Thermo Fisher Scientific Inc. (Waltham, MA, USA)
NanoDrop™ 2000c Spectrophotometer	Thermo Fisher Scientific Inc. (Waltham, MA, USA)

Consumables

Name	Provider
13 ml tube (100x16 mm, transparent, PP)	Sarstedt AG & Co. KG (Nümbrecht, Germany)
Bacterial Cell Spreaders (L-shaped)	Carl Roth (Karlsruhe, Germany)
Inoculation loops (1 µl)	Sarstedt AG & Co. KG (Nümbrecht, Germany)

Media, solutions and reagents

Name	Provider
LB-Media (Lennox)	Carl Roth (Karlsruhe, Germany)
Bacteriological Agar, for molecular biology (A5306-250G)	Sigma-Aldrich (St. Louis, MO, USA)
Ampicillin sodium salt	Carl Roth (Karlsruhe, Germany)

Name	Components	Provider
Quantum Prep™ Plasmid Midiprep Kit	Cell Resuspension Solution Cell Lysis Solution Neutralization Solution Quantum Prep matrix Midiprep Wash Buffer Spin columns and caps 2 ml microcentrifuge tubes	BIO-RAD Laboratories (Hercules, CA, USA)

Bacteria

Name	Provider
XL1-Blue Competent Cells (200249)	Aligent Technologies (Santa Clara, CA, USA)

2.2.1 Transformation

The competent bacteria were received from their storage at -70° C and thawed on ice. Then, 100 µl of bacterial suspension was added together with 1 µl of the intended plasmid into a cooled 13 ml tube, gently flicked and then incubated on ice for 20 min. Next, heat shock transformation was induced by placing the microbiology tube into a 42° C shaking water bath for exactly 45 sec. Then again, the mixture was incubated on ice for 2 min. Afterwards, 900 µl of LB medium, prewarmed at 42° C, was added and the bacterial suspension then incubated in the benchtop orbital shaker at 37° C for 60 min. Using a bacterial cell spreader or an inoculation loop, a small volume of the concentrated bacterial suspension was spread evenly onto a prewarmed 10 cm agar plate containing 50 µg/ml ampicillin. This was incubated at 37° C for 18 h.

2.2.2 Inoculation

Into a 13 ml tube 5 ml LB medium and 5 µl ampicillin were added. From the agar plate one isolated colony was selected against a dark background and then transferred into the tube using a pipette tip. This was incubated on the benchtop orbital shaker at 37° C for 6 h.

Into a sterile 500 ml glass bottle 100 ml of prewarmed LB medium and 100 µl ampicillin were added. Then, the bacterial suspension of the incubated tube was carefully transferred into the glass bottle. This was incubated with a loosely screwed on lid overnight on the benchtop orbital shaker at 37° C.

2.2.3 Plasmid isolation

The plasmid isolation was conducted using the Quantum Prep™ Plasmid Midiprep Kit by BIO-RAD and in accordance with the corresponding protocol. The overnight bacteria culture was poured into a sterile centrifuge bottle and then centrifuged at 3 000 x g for 5 min in the Sorvall® RC-5C Plus Superspeed Centrifuge for the bacteria to be spun down. The supernatant was discarded, and 5 ml of Cell Resuspension Solution was added. After vortexing vigorously to resuspend the cell pellet, 5 ml of Cell Lysis Solution was added, and the contents of the centrifuge bottle were mixed gently by inverting it. Next, 5 ml of Neutralization Solution was added and again mixed gently. The lysate suspension was then centrifuged at 7 500 x g for 10 min and the supernatant carefully transferred into a new bottle. The precipitate was discarded. To the lysate 1 ml of vortexed Quantum Prep matrix was added and gently mixed. It was centrifuged at 7 500 x g for 2 min and the supernatant was discarded. The pelleted matrix was resuspended with 10 ml of Midiprep Wash Buffer. The resuspended matrix was centrifuged again at 7 500 x g for 2 min and the supernatant wash buffer was discarded. The pelleted matrix was resuspended with 600 µl of Midiprep Wash Buffer and transferred into a Spin Column that was placed inside a 2 ml Collection Tube. Next, it was spun for 1 min at 13 000 x g in a microcentrifuge, then the wash buffer at the bottom of the collection tube was discarded. After adding another 500 µl of wash buffer into the Spin Column, it was again centrifuged for 1 min at 13 000 x g and the wash buffer was discarded. Another centrifugation was carried out at 13 000 x g for 2 min to remove any residual fluid from the matrix. The Spin Column

was then transferred into a new collection tube and 400 µl of H_2O dd was added to elute the plasmid DNA from the matrix. This was centrifuged at 13 000 x g for 2 min, then the Spin Column could be discarded. The collection tube now contained the plasmid DNA and using the NanoDrop spectrophotometer its concentration and purity was assessed. The isolated plasmid DNA was stored at -20° C.

2.3 Western Blotting

Technical Equipment

Name	Provider
SONOPLUS ultrasonic homogenizer HD 2070	Bandelin (Berlin, Germany)
Heraeus™ Biofuge™ fresco Microcentrifuge	Thermo Fisher Scientific Inc. (Waltham, MA, USA)
Tecan Sunrise™ Plate Reader	Tecan Group (Männedorf, Switzerland)
XFluor4 Software	Tecan Group (Männedorf, Switzerland)
Microsoft® Excel Office 2019	Microsoft Corporation (Redmond, WA, USA)
Dry Block Heating System QBD2	Grant (Cambridge, UK)
IKA® Vibrax® VXR basic Shaker	IKA Werke (Staufen, Germany)
PowerPac™ HC power supply	BIO-RAD Laboratories (Hercules, CA, USA)
Mini-PROTEAN® 3 Cell	BIO-RAD Laboratories (Hercules, CA, USA)
Mini Trans-Blot® Electrophoretic Transfer Cell	BIO-RAD Laboratories (Hercules, CA, USA)
Intelli-Mixer™ RM-2L	ELMI (Riga, Latvia)
Amersham™ ImageQuant™ 800 Western blot imaging systems	Cytiva (Malborough, MA, USA)
ImageQuant™ TL Software	Cytiva (Malborough, MA, USA)
GraphPad Prism 9 Software	GraphPad Software, Inc. (Boston, MA, USA)

Consumables

Name	Provider
Amersham™ Hybond™ PVDF membrane	Cytiva (Malborough, MA, USA)

Solutions and reagents

Name	Provider
Precision Plus Protein™ Standard All Blue	BIO-RAD Laboratories (Hercules, CA, USA)
Cycloheximide (CHX) (CAS-Nº. 66-81-9)	Carl Roth (Karlsruhe, Germany)

Name	Ingredients	
RIPA buffer	NaCl 150 mM	438,3 mg
	Tris-HCl 50 mM	394,0 mg
	Nonidet P 40	500,0 mg
	Deoxycholic acid sodium salt	125,0 mg
	SDS	50,0 mg

	H_2O dd	ad 50 ml
Lysis Buffer	RIPA buffer PMSF 100 mM NaF 200 mM Na_3VO_4 200 mM Proteasome inhibitor MG-132 20 µM (Santa Cruz Biotechnology, Dallas, TX, USA)	1 ml/sample 10 µl/sample 5 µl/sample 5 µl/sample 40 µl/sample
Bradford Solution	H2O dd ROTI®-Quant (Carl Roth, Karlsruhe, Germany)	1 ml/sample 250 µl/sample
3X SDS-PAGE Loading buffer	0,5 M Tris-HCl pH 6,8 SDS Glycerol Bromophenol blue H_2O dd	37,5 ml 6,0 g 30,0 ml 15,0 mg ad 100 ml
3X SDS-PAGE Loading buffer *prepared for use*	3X SDS-Page Loading Buffer DTT	20 µl/sample 2 µl/sample
Separation Gel 7,5 % (2 Gels)	30 % PAA 1,5 M Tris-HCl pH 8,8 10 % SDS H_2O dd *directly before use* TEMED APS 10 %	5 ml 3,75 ml 150 µl 6,1 ml 15 µl 75 µl
Stacking Gel (2 Gels)	30 % PAA 1,25 M Tris-HCl pH 6,8 10 % SDS H_2O dd *directly before use* TEMED APS 10 %	1,28 ml 750 µl 75 µl 5,25 ml 15 µl 75 µl
Electrophoresis Buffer (10X)	Tris-Base Glycine SDS H_2O dd	30 g 144 g 10 g ad 1 000 ml
Electrophoresis Buffer	Electrophoresis Buffer (10X) H_2O dd	100 ml ad 1 000 ml
Blotting Buffer (5X)	Tris-Base Glycine H_2O dd	15,17 g 72,9 g ad 1 000 ml
Blotting Buffer	Blotting Buffer (5X) MeOH dd H_2O dd	200 ml 200 ml ad 1 000 ml
TBS-T	Tris-Base NaCl	3,0 g 11,1 g

	Tween 20	1 ml
	H_2O dd	ad 1 000 ml
Blocking Solution with 5% BSA	Bovine Serum Albumin (Carl Roth, Karlsruhe, Germany)	2,5 g
	TBS-T	ad 50 ml

Name	Components	Provider
SuperSignal™ West Pico PLUS Chemiluminescent Substrate Kit	SuperSignal™ West Pico PLUS Luminol/Enhancer Solution SuperSignal™ West Pico PLUS Stable Peroxide Solution	Thermo Fisher Scientific Inc. (Waltham, MA, USA)
SuperSignal™ West Femto Maximum Sensitivity Substrate Kit	SuperSignal™ West Femto Luminol/Enhancer Solution SuperSignal™ West Stable Peroxide Solution	Thermo Fisher Scientific Inc. (Waltham, MA, USA)

Primary antibodies

Target	Source	Dilution	Provider
HA-tag (#3724)	rabbit	1: 1 000	Cell Signaling Technology Europe B.V. (Frankfurt am Main, Germany)
Myc-tag (#2276)	mouse	1: 1 000	Cell Signaling Technology Europe B.V. (Frankfurt am Main, Germany)
β-Actin (#8457)	rabbit	1: 1 000	Cell Signaling Technology Europe B.V. (Frankfurt am Main, Germany)

Secondary antibodies

Antibodies	Dilution	Provider
Amersham™ ECL™ Anti-rabbit IgG, HRP-linked, from donkey (NA934-1ML)	1,3 µl in 15 ml in TBS-T	Cytiva (Malborough, MA, USA)
Amersham™ ECL™ Anti-mouse IgG, HRP-linked, from sheep (NA931-1ML)	1,3 µl in 15 ml in TBS-T	Cytiva (Malborough, MA, USA)

2.3.1 Preparation and Treatment for half-life experiments

KEAP1-/- MEF cells were seeded on a 12 Well Cell Culture Plate containing ~ 60 000 cells in 1 ml of growth media per well. After about 24 h of incubation at 37° C and 5 % CO2, cells were either transfected with EGFP-Myc-WT-NRF2 or EGFP-Myc-TM-NRF2. On a separate cell culture plate cells were not only transfected with EGFP-Myc-WT-NRF2 or EGFP-Myc-TM-NRF2, but also co-transfected with *FBXW11* siRNA to knock down expression of β-TrCP2. The second day after transfection the old growth media containing the transfection mix was removed and replaced with

fresh growth media containing 50 µM of cycloheximide for 60, 30, 10 or 0 min. Following treatment with cycloheximide, which is an inhibitor of *de novo* protein synthesis used for investigating protein stability, cells were immediately lysed.

2.3.2 Cell Lysis and Protein Extraction

Samples were kept on ice during the whole procedure and lights were dimmed due to light sensitive MG-132 within the lysis buffer mix. First, the medium was removed, and the cells washed with 1 ml PBS per well. Then, 100 µl of the lysis buffer was added to each well, the cells were scraped off the surface with a cell scraper and transferred into an Eppendorf tube. In order to complete the lysis and homogenize the cell material the samples were each sonicated. Following 15 min of spinning at 17 000 x g and 4° C in the microcentrifuge, the supernatant containing the solubilized proteins was transferred into a new Eppendorf tube. Bradford assay was performed as previously described (https://www.antibody-creativebiolabs.com/protein-concentration-concentration-determination.htm).

2.3.3 Denaturation

In accordance with the results of the Bradford assay the respective amount of lysis buffer was added to the corresponding amount of cell lysate with uniform protein content. Then the samples were each mixed with 3X SDS-Page Loading Buffer plus 10 % DTT. After a quick spin they were incubated at 95° C for 5 min on a dry block heating system, then vortexed and spun again. At this step the samples could either be stored at -20° C or immediately subjected to electrophoresis.

2.3.4 SDS-PAGE

Sodium dodecyl sulfate-polyacrylamide gel electrophoresis (SDS-PAGE) is a method used to separate proteins by their molecular mass. Denatured proteins, which are treated with SDS to achieve a consistent charge : mass ratio, migrate through a polyacrylamide gel within an electric field.

Usually, gels were prepared a day in advance using the Mini-PROTEAN® 3 Cell system from BIO-RAD. First, for one gel two well cleaned glass plates were assembled within a casting frame to form a gel cassette, which was fixated by a casting stand. Then, the separation gel containing 7,5 % polyacrylamide was prepared, filled in between the glass plates and covered with 1 ml H_2O dd. After ca. 1 h the polymerization was finished and the water could be removed. The stacking gel was prepared and added on top. A comb was carefully inserted between the glass plates into the stacking gel. Lastly, after another hour the stacking gel too was polymerized and the gel cassette containing the gel could be removed from the casting frame and stored at 4° C.

Gel electrophoresis was also performed using the Mini-PROTEAN® 3 Cell system from BIO-RAD. First, the gel cassette was attached to an electrode assembly and fixated within a clamping frame, which was then placed inside the electrophoresis chamber. The electrophoresis buffer was prepared and filled into the chamber. After the careful removal of the comb, the slots were rinsed with electrophoresis buffer and then ready for loading. First though, should the protein samples have been

stored at -20° C beforehand they were again boiled at 95° C for 5 min, then vortexed and centrifuged. Next, 20 µg of each denatured protein sample was loaded into the slots of the gel. Additionally, 7,5 µl of Precision Plus Protein™ Standard All Blue protein ladder marker was added into a separate slot. The electrophoresis chamber was closed with a lid, all electrode plugs correctly assembled and connected with the PowerPac™ HC power supply (Fig. 8). Electrophoresis was performed at 20-40 mA and during the run its progress was regularly checked upon. The SDS-PAGE was considered finished when the blue front of the samples had reached the bottom of the gel.

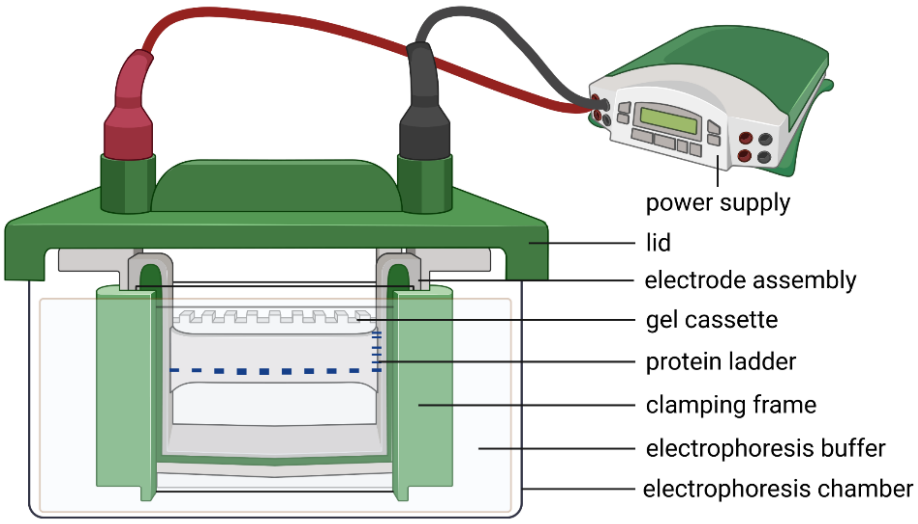

Figure 8 **Assembly of the Mini-PROTEAN® 3 Gel Electrophoresis module**
Figure created with BioRender.com.

2.3.5 Blotting

In order to enable detection, the separated proteins were now transferred from the gel onto a PVDF membrane using the Mini Trans-Blot® Electrophoretic Transfer Cell system. At the beginning, the membrane must be activated. Therefore, it was first put into methanol for 45 sec, then washed with blotting buffer for 5 min under rocking conditions on a shaker. The subsequent steps were conducted within ca. 1 000 ml of blotting buffer as to always keep the materials wet. First, the gel containing the separated proteins was carefully detached from the glass plates, then filter paper and fiber pads were soaked and a "blotting sandwich" was prepared. For this the gel holder cassette was filled in the following order from the black side: two fiber pads, two filter papers, the gel, the activated membrane, one filter paper and one fiber pad (Fig. 9A). Finally, after removing any possible air bubbles, the cassette was closed. It was then put into the electrode module and placed into the blotting tank alongside a box containing frozen water for cooling. The blotting tank was filled with blotting buffer, the lid closed, and all plugs assembled and connected with the PowerPac™ HC power supply (Fig. 9B). The transfer was performed at 4° C at either 100 V for 90 min or 30 V for 14 h.

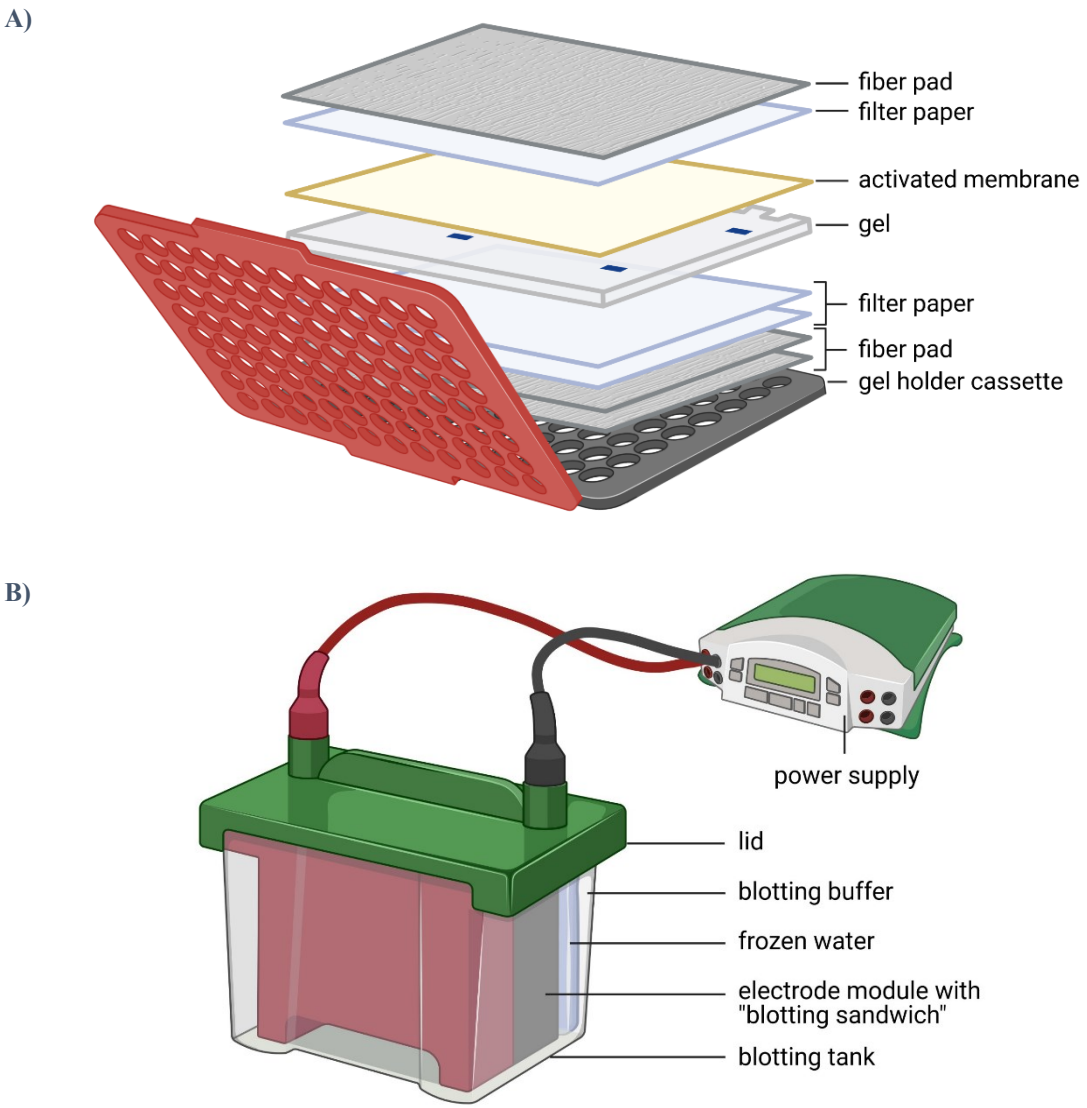

Figure 9 **(A) Assembly of a "blotting sandwich", (B) Assembly of the Mini Trans-Blot® Electrophoretic Transfer module**
Figure created with BioRender.com.

2.3.6 Blocking, treatment and immunodetection

After finishing the transfer, the membrane was removed from the "blotting sandwich" using forceps, put into methanol for 5 sec and then left to dry for 10-12 min. During this step and all the following the side of the membrane containing the proteins never came into contact with any surfaces. Next, the membrane was put into methanol for 45 sec, into H_2O dd for 5 sec and then washed in TBS-T for 5 min under rocking conditions. Afterwards, the membrane was placed into 25 ml of blocking solution containing 5 % BSA for 30-60 min under rocking conditions at room temperature.

Primary antibody solutions were either freshly prepared or thawed. After blocking was completed, the membrane was washed in TBS-T three times for 5 min, then carefully placed into a 50 ml Screw Cap Tube containing 15 ml of primary antibody solution. Lastly, the tube rotated overnight at 4° C

on the Intelli-Mixer™ RM-2L. The next day, the membrane was washed in TBS-T three times for 5 min. It was then added into a 50 ml Screw Cap Tube containing 15 ml of secondary antibody solution and rotated for 1 h at 4° C. Then the membrane was again washed in TBS-T three times for 5 min.

In preparation for immunodetection a working solution was made that consisted in equal parts of SuperSignal™ West Pico PLUS Luminol/Enhancer Solution and SuperSignal™ West Pico PLUS Stable Peroxide Solution. If necessary due to receiving only weak signals during detection, a working solution was prepared that additionally contained equal amounts of the reagents from the SuperSignal™ West Femto Maximum Sensitivity Substrate Kit. Each membrane was evenly coated with 2 ml of the working solution. Preparation of the working solution and coating of the membrane were conducted under dimmed lighting since the utilized reagents are light sensitive. Subsequently after coating, the membranes were analyzed with the Amersham ImageQuant™ 800 Western blot imaging systems. Afterwards the membrane was again washed three times in TBS-T and stored at 4° C. Densitometric evaluation was performed using ImageQuant™ TL Software and statistical analysis as well as graphing was conducted with GraphPad Prism 9 Software.

2.4 Proximity Ligation Assay (PLA)

The PLA method has the objective of examining and visualizing the *in situ* protein-protein interactions of two specific proteins. For this purpose, cells must first be fixated on microscope slides and permeabilized. They are then incubated with two sets of primary antibodies that are each specific for one of the two target proteins. Next, secondary antibodies conjugated with DNA oligos are added. After addition of hybridizing connector oligos, a ligase forms them into a circular DNA template – if the secondary antibodies are in close enough proximity. Then, a polymerase uses the secondary antibody´s DNA oligos as a primer for rolling circle amplification and produces an elongated single strand of DNA still tethered to the protein via the secondary antibody. Finally, fluorescence detectable oligos are added which hybridize with the amplified DNA strand thus making the interacting proteins visible under a microscope (Fig. 10).

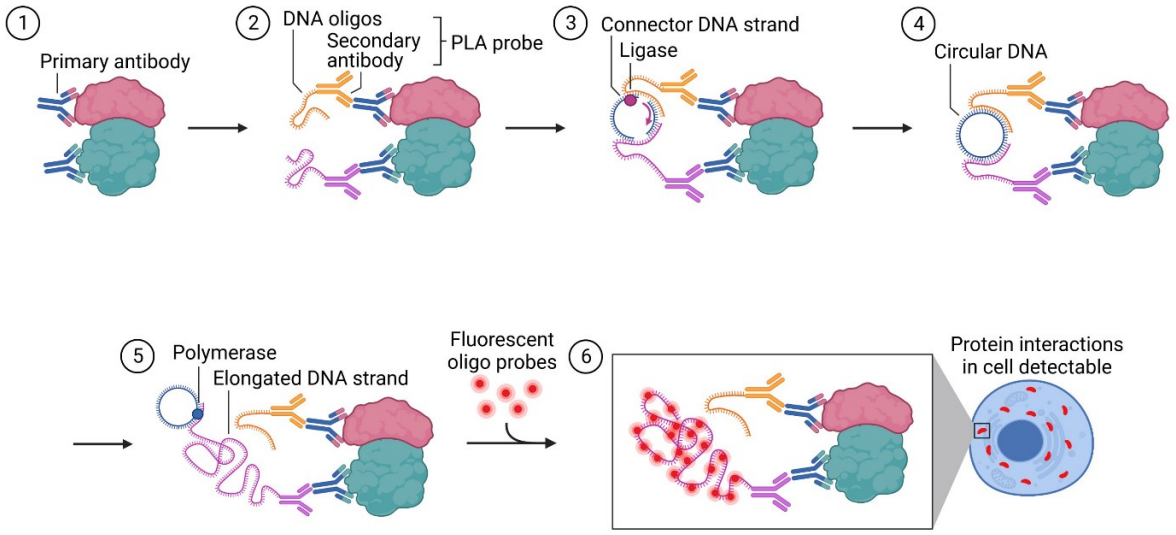

Figure 10 **Schematic illustration of the detection and visualization of protein interactions during PLA**
Figure created with BioRender.com.

Technical equipment

Name	Provider
Leica DMi8 Microscope	Leica Microsystems (Wetzlar, Germany)
Leica Application Suite X (LAS X)	Leica Microsystems (Wetzlar, Germany)

Consumables

Name	Provider
Microscope slides (clear, cut edges, plain end)	VWR International GmBH (Randor, PA, USA)

Solutions and reagents

Name	Provider
Gelatin from porcine skin, gel strength 80-120g Bloom, Type A (G6144-100G)	Sigma-Aldrich (St. Louis, MO, USA)
Formaldehyde solution ROTIPURAN® 37 %, p.a., ACS (4979.1) (CAS-Nº. 50-00-0)	Carl Roth (Karlsruhe, Germany)
Triton X-100, for molecular biology (CAS-Nº. 9002-93-1)	Sigma-Aldrich (St. Louis, MO, USA)
Duolink® in Situ PLA® Probe Anti-Rabbit PLUS (DUO92002)	Sigma-Aldrich (St. Louis, MO, USA)
Duolink® in Situ PLA® Probe Anti-Mouse MINUS (DUO92004)	Sigma-Aldrich (St. Louis, MO, USA)
Duolink® Antibody Diluent	Sigma-Aldrich (St. Louis, MO, USA)
Duolink® Wash Buffer A	Sigma-Aldrich (St. Louis, MO, USA)
Duolink® Wash Buffer B	Sigma-Aldrich (St. Louis, MO, USA)
5X Duolink® Ligation Buffer	Sigma-Aldrich (St. Louis, MO, USA)
Duolink® Ligase (1 U/µl)	Sigma-Aldrich (St. Louis, MO, USA)
5X Duolink® Amplification Buffer	Sigma-Aldrich (St. Louis, MO, USA)
Duolink® Polymerase (10 U/µl)	Sigma-Aldrich (St. Louis, MO, USA)
Duolink® Mounting Media with DAPI	Sigma-Aldrich (St. Louis, MO, USA)

2.4.1 Preparation, treatment and fixation

Coverslips were put into the wells of a 12 Well Cell Culture Plate and then coated with 500 µl 0,1 % gelatin/PBS. After 30 min, 0,1 % gelatin/PBS was removed and ~ 60 000 KEAP1-/- MEF cells were seeded on the coverslips in 1 ml of growth media. After about 24 h of incubation at 37° C and 5 % CO_2, cells were transfected with the respective plasmids. The second day after transfection fresh growth media containing 10 µM of the proteasome inhibitor MG-132 was added in the presence or absence of 50 µM A-769662. Since A-769662 and MG-132 are light sensitive, this step was performed with dimmed lighting. Afterwards, cells were incubated for another 4 h, then the growth media was removed, and the cells washed with 1 ml of PBS. Finally, cells were fixated through exposing them to 500 µl of 4 % paraformaldehyde/PBS per well for 15 min at room temperature. Lastly, cells were washed three times with PBS and could then be stored in PBS at 4° C.

2.4.2 Permeabilization and Blocking

After removing the PBS, the fixated cells were treated with 1 ml of a 1:1 000 dilution of Triton X 100/PBS per well for 90 sec in order to achieve permeabilization. Then, using forceps, the coverslips with the fixated cells were removed from their respective wells and placed onto 2-3 drops of blocking solution, which were prepared in advance on the labeled lid of the cell culture plate.

Attention should be paid to having the surface containing the cells face the blocking solution and being entirely covered by it. The coverslips were incubated in a humidity chamber in the B 15 Compact Incubator at 37° C for 60 min.

2.4.3 Primary Antibody and PLA Probe incubation

The Duolink® Antibody Diluent was vortexed and used to prepare a 1:1 000 antibody dilution containing both primary antibodies (HA-tag for β-TrCP and Myc-tag for NRF2, see Ch. 2.3). The coverslips were retrieved from the incubator and washed with 1 ml of PBS in their respective wells of the cell culture plate. Next, for each coverslip a drop of 100 µl antibody dilution was prepared again on top of the lid of the cell culture plate and the coverslips placed onto the drops. This was incubated overnight at 4° C. The following day, the coverslips containing the cells were each washed twice in 1 ml of Duolink® Wash Buffer A in their respective wells for 5 min. The Duolink® PLA Probes PLUS and MINUS, which contain the rabbit and mouse secondary antibodies conjugated with oligos respectively, were vortexed and a 1:5 PLA probe dilution containing both PLA probes was prepared using the Duolink® Antibody Diluent. For each coverslip a drop of 40 µl PLA probe dilution was put on the lid of the cell culture plate and the coverslips placed onto these drops. This was incubated in a humidity chamber at 37° C for 60 min.

2.4.4 Ligation

The coverslips were each washed twice in 1 ml of Duolink® Wash Buffer A in their respective wells for 5 min. The 5X Duolink® Ligation Buffer was diluted 1:5 with H_2O dd and vortexed, subsequently the ligase was thawed and added at the ratio 1:40. This ligation solution was mixed gently and for each coverslip a drop of 40 µl was put on the lid of the cell culture plate and the coverslips placed onto these drops. This was incubated in a humidity chamber at 37° C for 30 min.

2.4.5 Amplification

The coverslips were each washed twice with 1 ml of Duolink® Wash Buffer A in their respective wells for 5 min. The 5X Duolink® Amplification Buffer was diluted 1:5 with H_2O dd and vortexed, afterwards the polymerase was added at the ratio 1:80. This amplification solution was gently mixed and for each coverslip a drop of 40 µl was put on the lid of a cell culture plate and the coverslips placed onto the drops. Since the Duolink® Amplification Buffer is light sensitive, these steps were performed with dimmed lighting. The coverslips were incubated with the amplification solution in a humidity chamber at 37° C for 100 min.

2.4.6 Final washes and preparation for imaging

The coverslips were each washed twice in 1 ml of Duolink® Wash Buffer B in their respective wells for 10 min. The Duolink® Wash Buffer B was diluted 1:100 with H_2O dd and the coverslips were washed again in 1 ml of the diluted Duolink® Wash Buffer B for 1 min. Lastly, the coverslips were mounted on labeled microscope slides each using 2 drops of Duolink® Mounting Media with DAPI. Due to light sensitive reagents, these steps were also conducted with dimmed lighting. The

microscope slides now contained the cells and were ready for imaging. They could be stored short-time at 4° C or for up to 6 months at -20° C.

2.4.7 Analysis via confocal microscopy

The protein-protein interaction within the cells was analyzed and z-stacks were obtained using a Leica DMi8 inverted confocal microscope. For image analyzation and documentation purposes, the Leica Application Suite X (LAS X) 3.1.2 software was used.

2.5 mRNA detection

Technical equipment

Name	Provider
Heraeus™ Fresco™ 21 Microcentrifuge	Thermo Fisher Scientific Inc. (Waltham, MA, USA)
Heraeus™ Labofuge™ 400 Centrifuge	Thermo Fisher Scientific Inc. (Waltham, MA, USA)
DNA/RNA UV-Cleaner box UVT-S-AR	Biosan Medical-Biological Research & Technologies (Riga, Latvia)
C1000™ Thermal Cycler	BIO-RAD Laboratories (Hercules, CA, USA)
LightCycler® 480 System	Roche (Basel, Switzerland)

Consumables

Name	Provider
Filter tips (10 µl, 100 µl, 1000 µl)	Sarstedt AG & Co. KG (Nümbrecht, Germany)
Multiply®-µStrip Pro 8-strip	Sarstedt AG & Co. KG (Nümbrecht, Germany)
96 Well PCR Plate for LightCycler	Sarstedt AG & Co. KG (Nümbrecht, Germany)
Transparent adhesive PCR film	Sarstedt AG & Co. KG (Nümbrecht, Germany)

Solutions and reagents

Name	Components	Provider
innuPREP RNA Mini Kit 2.0	Lysis Solution RL Washing Solution HS (conc.) Washing Solution LS (conc.) RNase-free Water Spin Filter D Spin Filter R Receiver tubes Elution tubes	AJ Innuscreen GmbH (Berlin, Germany)
High-Capacity cDNA Reverse Transcription Kit	10X RT Buffer 25X dNTP Mix (100 mM) 10X RT Random Primers MultiScribe™ Reverse Transcriptase RNase Inhibitor Nuclease-free H_2O	Thermo Fisher Scientific Inc. (Waltham, MA, USA)
2X Luna® Universal qPCR Master Mix		New England Biolabs (Ipswich, MA, USA)

Primers

Name	Provider
TBP-Primer (fwd: TCTACCGTGAATCTTGGCTGT, rev: GTCCGTGGCTCTCTTATTCTCA)	Invitrogen, via Thermo Fisher Scientific Inc. (Waltham, MA, USA)
Gclc-Primer (fwd: TGGCCACTATCTGCCCAATT, rev: GTCTGACACGTAGCCTCGGTAA)	Invitrogen, via Thermo Fisher Scientific Inc. (Waltham, MA, USA)

2.5.1 Preparation and treatment

Cells were seeded on a 12 Well Cell Culture Plate containing ~ 60 000 KEAP1-/- MEF cells in 1 ml of growth media per well. After about 24 h of incubation at 37° C and 5 % CO_2, cells were transfected with the respective NRF2 forms with co-transfection of β-TrCP2. The second day after transfection the cells were treated with or without A-769662. Since A-769662 is light sensitive, this step was performed with dimmed lighting. Cells were again incubated for either 4 h or 24 h before RNA isolation was performed.

2.5.2 Cell Lysis and RNA isolation

The following steps were performed using the protocol, consumables and reagents provided by the innuPREP RNA Mini Kit 2.0 by AJ Innuscreen. Further, during all steps the use of RNase-free filter tips was required as to not compromise the isolated RNA. At the beginning, the medium was removed, and the cells washed with 1 ml PBS per well. Then, 400 µl of Lysis Solution RL was added to the respective wells and the cells detached from the surface using a cell scraper. The cell lysate was resuspended within the well, transferred into elution tubes and resuspended again after 2 min. After 3 min of incubation at room temperature, the lysates could now be stored at -80° C.

In order to selectively remove genomic DNA, the lysed samples were transferred into a Spin Filter D, which was placed into a receiver tube. Next, the samples were centrifuged at 11 000 x g for 2 min in the Heraeus™ Fresco™ 21 Microcentrifuge, afterwards the Spin Filter D binding the DNA was discarded. The filtrate containing the RNA was transferred into a Spin Filter R, which was placed into a new receiver tube. To each sample 400 µl of 70 % ethanol was added and well resuspended. Again, the samples were centrifuged at 11 000 x g for 2 min. The Spin Filter R, now binding the RNA, was retained and underwent the following washing steps. First, it was placed into a new receiver tube and 500 µl of Washing Solution HS (diluted 1:1 with 99 % ethanol) was added. Then, the samples were centrifuged at 11 000 x g for 1 min. Again, the Spin Filter R was placed into a new receiver tube, 700 µl of Washing Solution LS (diluted 1:4 with 99 % ethanol) was added and the samples centrifuged at 11 000 x g for 1 min. In a last washing step, the Spin Filter R was again placed into a new receiver tube, 700 µl of 80 % ethanol was added and the samples centrifuged at 11 000 x g for 1 min. Then, the Spin Filter R was again placed into a new receiver tube and centrifuged at

11 000 x g for 3 min to remove any residual fluid. To finally elute the RNA from the Spin Filter R, it was placed into an elution tube and 30 µl of RNase-free water was added. Then the samples were centrifuged at 11 000 x g for 1 min. Thus, the isolation of RNA was completed, and the acquired samples could be stored at -80° C.

2.5.3 cDNA synthesis

For the reverse transcription of the isolated RNA into cDNA, experiments were conducted using the High-Capacity cDNA Reverse Transcription Kit by Thermo Fisher Scientific. First though, the RNA concentration of the samples was measured, and their purity verified with the NanoDrop spectrophotometer. Then, using Excel, for each sample the required amount of isolated RNA-sample plus RNas-free water was calculated to achieve a concentration of 1 000 ng RNA in 10 µl water. The subsequent steps were performed in a DNA/RNA UV-Cleaner box with the reagents and samples on ice to keep them cooled. In accordance with the calculated ratios, the required amounts of sample and RNase-free water were added into the tubes of a Multiply®-µStrip Pro 8-strip and mixed. A Reverse Transcription Master Mix was prepared as per the user guide of the kit:

Component	Volume/ sample
10X RT Buffer	2.0 µl
25X dNTP Mix (100 mM)	0.8 µl
10X RT Random Primers	2.0 µl
MultiScribe™ Transcriptase	1.0 µl
RNase Inhibitor	1.0 µl
Nuclease-free water	3.2 µl

All components were gently mixed and to each sample 10 µl of the master mix was added. After careful resuspension and a quick spin in the Heraeus™ Labofuge™ 400 Centrifuge at 170 x g for 1 min, the samples were loaded into the C1000™ Thermal Cycler. The cDNA synthesis was performed in the thermal cycler under the following conditions:

1. 25,0° C for 10 min
2. 37,0° C for 120 min
3. 85,0° C for 5 min
4. 4,0° C forever

After the reverse transcription was completed, 30 µl of Nuclease-free water was added to the samples as to reach a final volume of 50 µl per tube and a cDNA concentration of approximately 20 ng/µl. The cDNA samples could be stored at -20° C.

2.5.4 Quantitative Polymerase Chain Reaction (qPCR)

In order to quantify the genes of interest of the previously obtained cDNA samples a qPCR assay was performed. PCR is used to replicate certain target regions of a cDNA strand. During one of its

cycles the cDNA first is heated to 95° C to denature, then the temperature is reduced as to allow specific primers to align with their target sequence and the polymerase to bind and translate the desired region of interest. In the qPCR technique during each amplification step a fluorescence dye intercalates into the double-stranded DNA which increases its fluorescence intensity. Thus, upon reaching a certain threshold level of cDNA, the fluorescence signal can be detected. The required number of PCR cycles to reach a detectable DNA concentration (Ct value) allows the quantification of the sample´s target gene.

All steps in preparation for the qPCR were performed on ice. First, the respective wells of a 96 Well PCR Plate were loaded with 2 µl of the cDNA samples and additionally, as a negative control, 2 µl of Nuclease-free water. Each sample was pipetted in duplicates for every tested gene. Then, for each required primer a qPCR master mix was prepared according to the Luna® Universal qPCR Master Mix Protocol by New England Biolabs as follows:

Component	Volume/ sample
2X Luna® Universal qPCR Master Mix	7.5 µl
10 µM specific Primer (forward and reverse)	1.5 µl
Nuclease-free water	4 µl

All components of the respective qPCR master mix were mixed gently and handled in consideration of the light sensitivity of the Luna® Universal qPCR Master Mix. Afterwards, 13 µl of the qPCR master mix containing the required primer was added to the respective cDNA samples and carefully resuspended. Finally, the PCR plate was sealed with adhesive PCR film, centrifuged at 2 000 x g for 3 min and inserted into the LightCycler® 480. The qPCR was run with the following settings: Denaturation at 95° C for 1 min and subsequently 45 amplification cycles, each with 15 sec of denaturation at 95° C followed by 30 sec of annealing at 60° C. The cycling program ended with a melting curve analysis (95° C for 15 sec, 55° C for 30 sec).

Data analysis was performed using the LightCycler® 480 Software and the relative target gene expression was determined with the $2^{-\Delta\Delta Ct}$ method using Excel. As per this calculation method, first the mean of the Ct values for every tested gene of each sample is calculated and normalized to the mean Ct value of the house keeping gene, viz. the TATA-box binding protein (*TBP*). The obtained ΔCt values are related by subtraction to the ΔCt values of a reference sample, e.g. untreated WT-NRF2 & β-TrCP2 cells, thus providing the ΔΔCt values. Since the ΔΔCt value of the reference sample is equal to 0, but in graphic representation its gene expression level is set to 1, the formula for determining the relative target gene expression levels must be $2^{-\Delta\Delta Ct}$. GraphPad Prism 9 Software was used for statistical analysis and creating graphs.

3 Results and discussion

3.1 NRF2 protein stability

The localization of the AMPK-dependent phosphorylation sites within or close to the Neh6 region, and thus the β-TrCP-interacting domain, suggests the phospho-sites to affect the degradation of NRF2. Thus, to examine the influence of these serine residues on NRF2 abundance, cells transfected with either the wild type (EGFP-Myc-WT-NRF2) or the mutated version of NRF2 (EGFP-Myc-TM-NRF2 with Ser374, 408 and 433 mutated to Ala) were subjected to half-life experiments to investigate whether protein stability will be affected.

Previous immunoblot assays conducted by Matzinger et al. 2020 have shown that WT- and TM-NRF2 display similar patterns of degradation in wild type MEF cells. This is presumably due to the dominating role of KEAP1 concerning NRF2 depletion that masks the influence of β-TrCP on the degradation of NRF2 [7]. Thus, the experiments presented in this master thesis were performed under KEAP1 knockout conditions.

3.1.1 AMPK-dependent phosphorylation sites affect NRF2 half-life

The impact of the AMPK-dependent serine residues on NRF2 protein stability was first examined by comparing degradation kinetics of WT- and TM-NRF2. For this reason, KEAP1-/- MEF cells were transiently transfected with either EGFP-Myc-WT- or EGFP-Myc-TM-NRF2 and then exposed to cycloheximide, an inhibitor of *de novo* protein synthesis, for different periods of time, thus allowing the observation of time-dependent NRF2 degradation. NRF2 protein abundance was determined using immunoblot analysis for Myc-tag, consequently guaranteeing the exclusive detection of transfected NRF2 while interference of endogenous NRF2 with the signal could be ruled out.

The results demonstrated that the protein levels of TM-NRF2 displayed higher stabilization and an extended half-life when compared with WT-NRF2 levels. Quantification analysis illustrates NRF2 stability in the triple mutated form in comparison to the wild type form (Fig. 11).

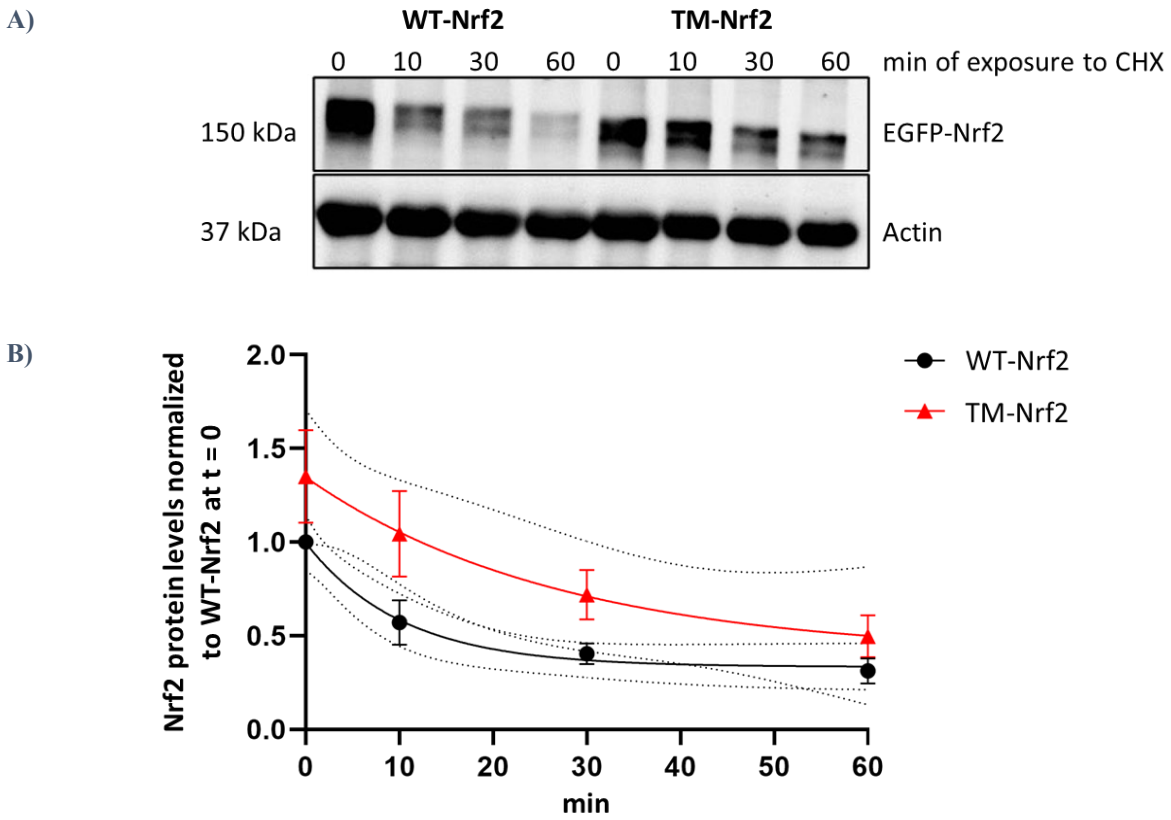

Figure 11 **NRF2 protein stability in KEAP1-/- MEF cells**
KEAP1-/- MEF cells were transfected with either EGFP-Myc-WT- or EGFP-Myc-TM-NRF2. They were exposed to 50 µM cycloheximide (CHX) for different amounts of time and subjected to immunoblot analysis for Myc-tag and β-Actin. (A) A representative blot and (B) quantification analysis relative to the WT-NRF2 signal at t = 0 are depicted. WT- and TM-NRF2 stability over time are illustrated as one-phase exponential decay curves, that were fitted to the data acquired by densitometric evaluation of the blots using the method of least squares (n = 9, means ± SEM, p = 0.0108). Figures kindly provided by Dr. Eleni Petsouki.

The mutation of the AMPK-dependent phospho-sites leads to stabilization of NRF2 in the respective KEAP1-/- MEF cells. Hence, these results indicate that the concerned phospho-sites in NRF2 play a role in mediating its degradation in a KEAP1-independent manner.

3.1.2 AMPK-dependent phosphorylation sites affect NRF2 degradation via β-TrCP2

The next step was to examine whether the detected effect of the phosphorylation sites on NRF2 stability is β-TrCP dependent. Therefore, KEAP1-/- MEF cells expressing WT- or TM-NRF2 were co-transfected with *FBXW11* siRNA. The *FBXW11* gene encodes for β-TrCP2, hence transfection with *FBXW11* siRNA triggers β-TrCP2 knockdown within the respective cells. This allows assessing whether the detected discrepancy in the degradation of WT-and TM-NRF2 depends on β-TrCP2.

The results show that under β-TrCP2 knockdown conditions the wild type and the triple mutant display similar kinetics of degradation in KEAP1-/- MEF cells. Quantification analysis demonstrates comparable WT- and TM-NRF2 protein levels from the beginning (t = 0), that exhibit a similar linear decline after exposure to the protein synthesis inhibitor cycloheximide (Fig. 12).

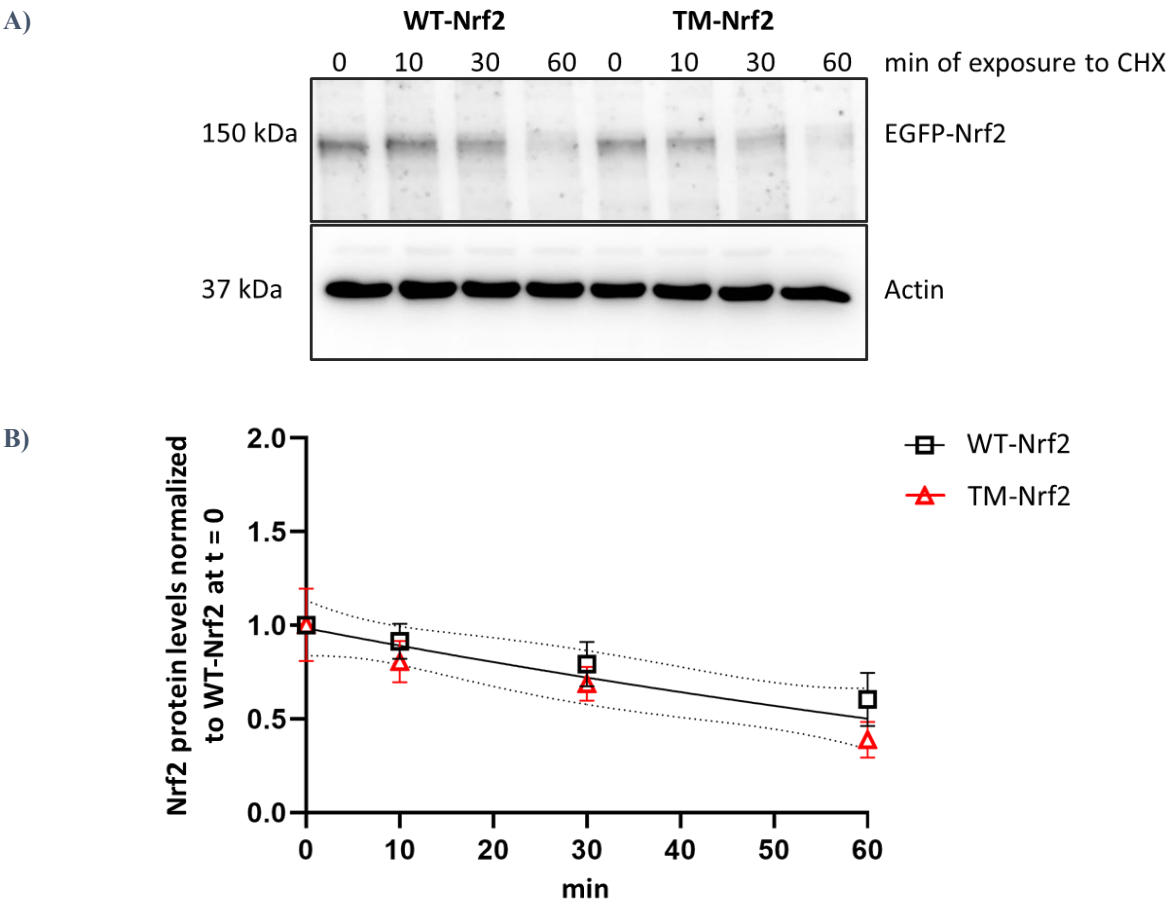

Figure 12 **NRF2 protein stability in KEAP1-/- MEF cells with β-TrCP2 KD**
KEAP1-/- MEF cells were transfected with either EGFP-Myc-WT- or EGFP-Myc-TM-NRF2 and co-transfected with *FBXW11* siRNA to induce β-TrCP2 knockdown. They were exposed to 50 µM cycloheximide (CHX) for different amounts of time and subjected to immunoblot analysis for Myc-tag and β-Actin. (A) A representative blot and (B) quantification analysis relative to the WT-NRF2 signal at t = 0 are depicted. WT- and TM-NRF2 stability over time are illustrated as one-phase exponential decay curves, that were fitted to the data acquired by densitometric evaluation of the blots using the method of least squares (n = 5, means ± SEM, p = 0.4852). Figures kindly provided by Dr. Eleni Petsouki.

These results show that the identified phospho-residues in NRF2 regulate the degradation of the protein in a β-TrCP2 dependent way under KEAP1-/- conditions (see Ch. 3.1.1), as the observed difference between WT- and TM-NRF2 stability is abolished under β-TrCP2 knockdown conditions. This suggests that the AMPK-dependent phospho-sites in NRF2 increase its degradation via β-TrCP2. Conversely, mutation of the respective serine residues seems to impede the β-TrCP2-mediated degradation of NRF2.

3.2 NRF2/β-TrCP protein interaction

To further elucidate how the AMPK-dependent phosphorylation sites affect the β-TrCP-mediated regulation of NRF2, protein interaction between NRF2 and β-TrCP2 has been examined by PLA comparing the wild type with the mutated version of NRF2. Moreover, to examine the phospho-sites´ effect on protein interaction in more detail and to investigate the role of AMPK on NRF2/ β-TrCP2 interaction, the protein interaction between NRF2 and β-TrCP2 was also studied in the presence of an AMPK activator. To exclude experimental artifacts, cells solely expressing either WT-NRF2, TM-NRF2, β-TrCP2 or pcDNA served as controls. Also, interaction was exclusively detected between transfected NRF2 and transfected β-TrCP2 since the Myc-tag of NRF2 and the HA-tag of β-TrCP2 served as the targets of the PLA primary antibodies. Each direct interaction of Myc-NRF2 and HA-β-TrCP2 was detected as a red signal under a fluorescence microscope. DAPI staining was used to visualize the nuclei of the cells (Fig. 13).

The results indicate that NRF2 interaction with β-TrCP2 was generally higher in cells expressing the wild type form of NRF2 than in those expressing the triple mutated version. Hence, mutation of the identified phospho-residues in NRF2 impeded its interaction with β-TrCP2 (Fig. 13A,B). Notably, in the presence of A-769662 the interaction of both forms of NRF2 with β-TrCP2 increased per se, especially in the nucleus. Still, cells transfected with WT-NRF2 and β-TrCP2 displayed a more pronounced nuclear interaction signal than TM-NRF2 transfected cells (Fig. 13B).

A)

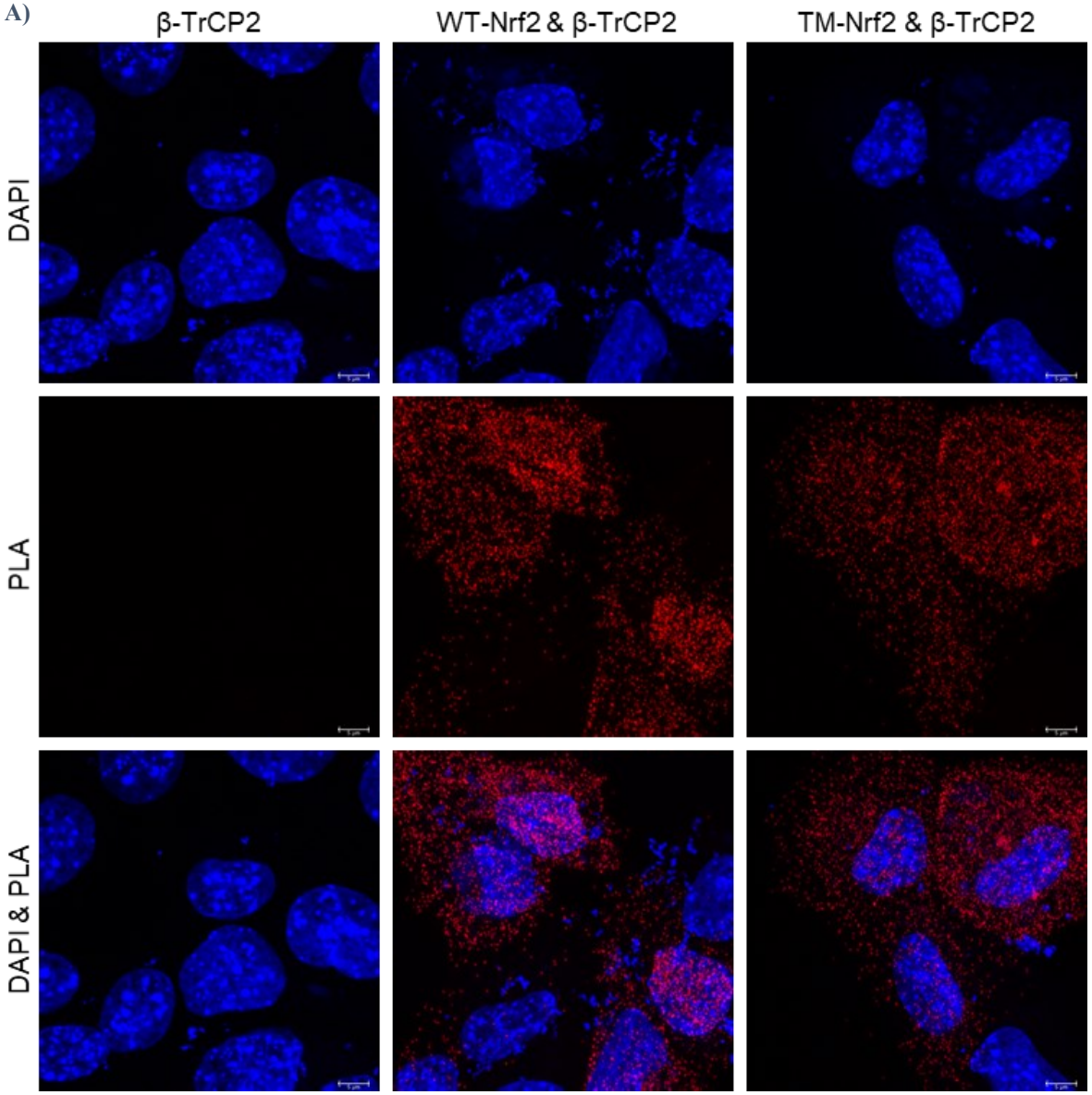

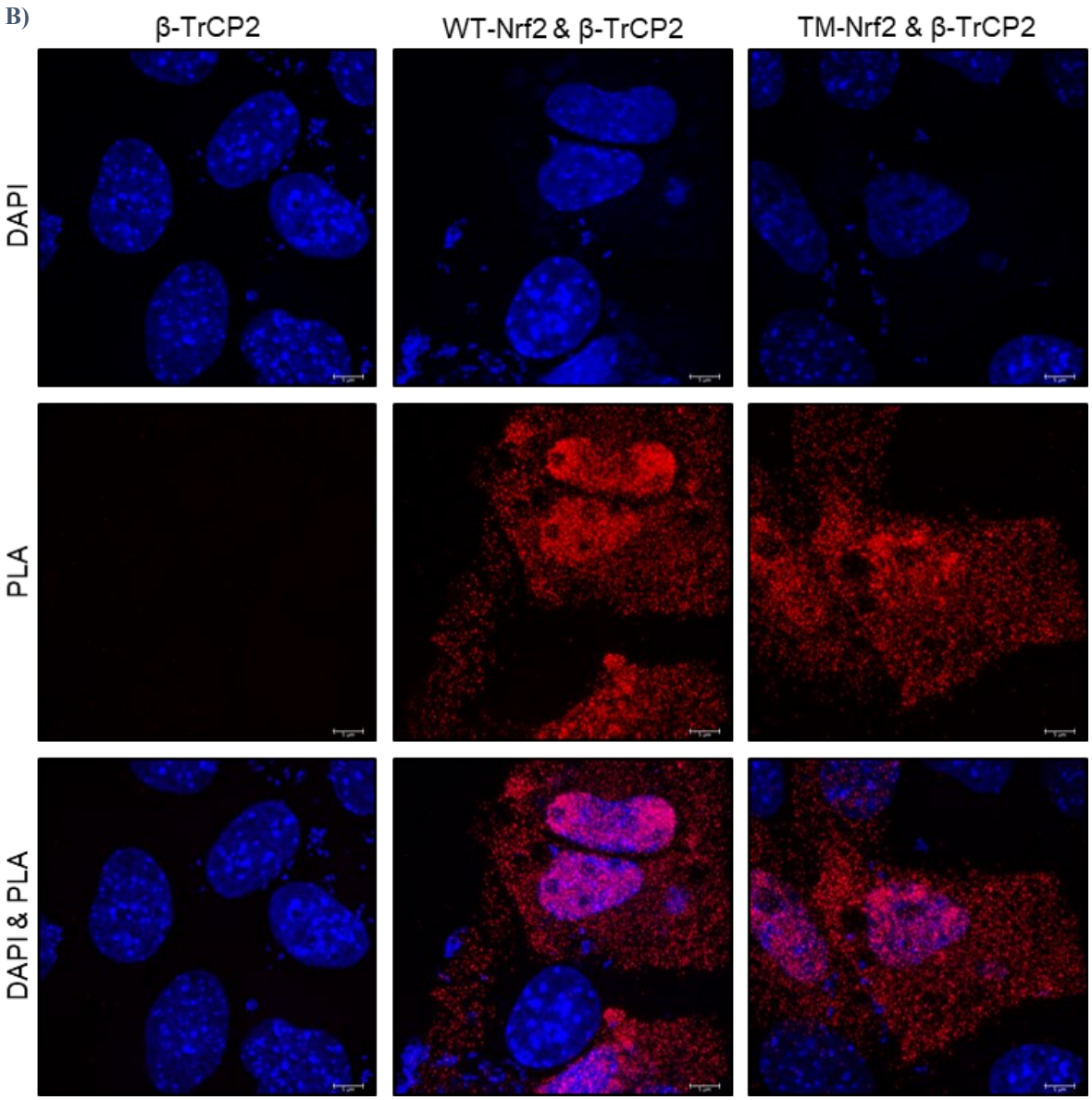

Figure 13 **NRF2/ β-TrCP2 interaction in KEAP1-/- MEF cells**

KEAP1-/- MEF cells were transfected with HA-β-TrCP2 together with either EGFP-Myc-WT- or EGFP-Myc-TM-NRF2. Control cells solely expressing HA-β-TrCP2 (A, B) or EGFP-Myc-WT-NRF2, EGFP-Myc-TM-NRF2 and pcDNA (data not shown) were prepared as well. Cells were exposed to 10 µM MG-132 for 4 h to accumulate NRF2 either (A) in the absence or (B) presence of 50 µM A-769662. They were then fixated with 4% paraformaldehyde, permeabilized and subjected to PLA assay. DAPI staining indicates the location of the nucleus and each red fluorescence signal visualizes an interaction between Myc-NRF2 and HA-β-TrCP2. Primary antibodies against Myc-tag and HA-tag were used in the PLA assay to represent interaction between transfected NRF2 and β-TrCP2 without interference of endogenous proteins. The control experiments with single HA-β-TrCP2 transfection affirm that there are no artificial PLA signals. Representative images obtained with LAS X software by Dr. Eleni Petsouki are depicted (scale bar 5 µm).

These findings confirm that the alleviated β-TrCP2-mediated degradation of TM-NRF2 discovered in the previous experiments (Ch. 3.1) is caused by reduced interactions of β-TrCP2 with the triple mutant. Hence, the AMPK-dependent phosphorylation sites in WT-NRF2 induce its degradation by facilitating the interaction between NRF2 and β-TrCP2.

Further, AMPK activation facilitated nuclear interaction between NRF2 and β-TrCP2 per se (Fig. 13B). These results may be explained by findings of Joo et al. 2016. They were the first to locate an AMPK-dependent phospho-site in NRF2 (Ser558) and discovered that the AMPK-triggered phosphorylation of this serine residue upon exposure to AICAR caused the accumulation of NRF2 in the nucleus of HEK cells [93]. The same may have occurred in our experiments. As a consequence, the nuclear accumulation of NRF2 led to elevated PLA signals in the nucleus of cells transfected with WT-NRF2 and β-TrCP2. Accordingly, TM-NRF2 also accumulated in the nucleus of the respective cells, but this was less detectable in the given experimental setting as TM-NRF2 has less interaction with β-TrCP2 and thus generates fewer PLA signals.

As discussed before (Ch. 1.5) research on the crosstalk between AMPK and NRF2 so far has shown for AMPK to mostly upregulate activity of NRF2. The AMPK-facilitated nuclear accumulation of NRF2 as observed in the PLA assay is another example of AMPK regulating NRF2 in a positive manner. However, the PLA results more particularly also confirm that the AMPK-dependent phospho-sites in NRF2 mediate its interaction with β-TrCP2. Consequently, this suggests a possible dual role of AMPK in the regulation of NRF2, specifically in a KEAP1-knockout background.

Previous studies have reported that GSK-3β facilitates the interaction of NRF2 with β-TrCP2, thus mediating its ubiquitination and subsequent degradation [24,47,48]. However, GSK-3, which has also been reported to be involved in regulating nuclear abundance of NRF2 [93,95], would not be expected to have any relevance under the given experimental conditions due to the following reasons: GSK-3 is enzymatically active only under resting conditions induced e.g. by serum starvation [32,49]. Yet, in the experimental setting of this thesis, cells were cultivated in 10 % fetal calf serum and therefore GSK-3 was repressed by the contained growth factors. Further, GSK-3 is known to be inhibited by AMPK [93], meaning that if the kinase had played a relevant part in our experiments, the addition of an AMPK activator would have downregulated GSK-3 activity and thus NRF2/ β-TrCP2 interaction. However, activation of AMPK showed the opposite effect.

Therefore, further investigation is needed in order to elucidate whether AMPK directly mediates the interaction of NRF2 with β-TrCP2 or primes NRF2 for another yet undiscovered kinase that promotes NRF2/ β-TrCP2 interaction.

3.3 NRF2-target gene expression

The effect of the AMPK-dependent phosphorylation sites on the β-TrCP2-mediated degradation of NRF2 raises the question whether this mechanism also affects the NRF2 target gene expression. For this reason, the gene expression of a prominent NRF2 target gene, viz. the gene encoding for the glutamate-cysteine ligase catalytic subunit (*Gclc*), was investigated. KEAP1-/- MEF cells, co-transfected with β-TrCP2 and either WT-NRF2 or TM-NRF2 were exposed to A-769662 for 4 h, and in another set for 24 h. Also, to determine the impact of AMPK activation, control experiments in the absence of A-769662 were performed for the respective amounts of time.

The 4 h experiments did not deliver any significant differences – neither for the cells with activated AMPK nor for the control cells (data not shown). The 24 h experiments however demonstrated differences between the target gene expression of cells co-transfected with the wild type and those co-transfected with the mutant version of NRF2. The results show that cells expressing TM-NRF2 display a significantly higher *Gclc* gene expression than those with WT-NRF2. This difference in expression regarding WT- and TM-NRF2 was detected in cells with activated AMPK as well as in those serving as controls. Though, regardless of the transfected NRF2 version, cells with AMPK activation exhibited generally higher *Gclc* mRNA levels than their respective non-activated counterparts (Fig. 14).

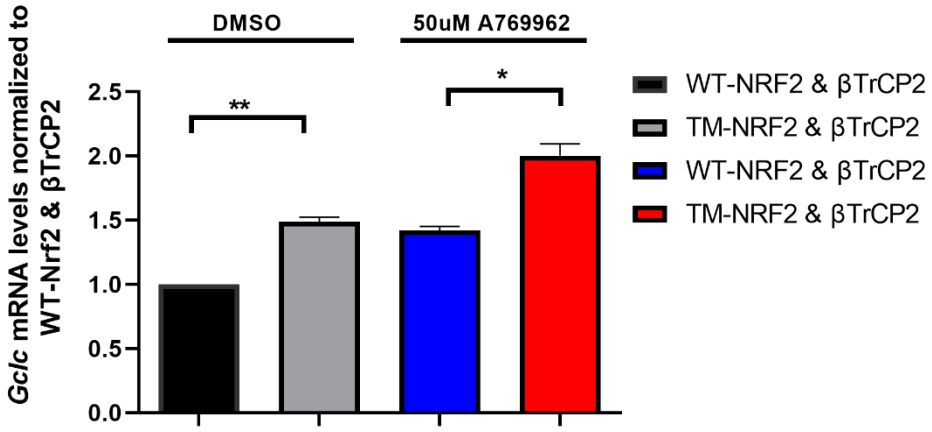

***Figure 14 Gclc* gene expression in KEAP1-/- MEF cells overexpressing NRF2 and β-TrCP2**
KEAP1-/- MEF cells were transfected with HA-β-TrCP2 together with either EGFP-Myc-WT- or EGFP-Myc-TM-NRF2 and treated with 50 µM A-769662 for 24 h. Untreated cells served as controls. RNA was extracted and the abundance of *Gclc* mRNA analyzed via qPCR. Control cells transfected with pcDNA (data not shown) confirm that endogenous *Gclc* mRNA levels are negligible compared to those of the cells overexpressing NRF2 and β-TrCP2. The bars depict the compiled *Gclc* mRNA levels normalized to the *Gclc* levels of untreated cells transfected with WT-NRF2 and β-TrCP2 (n = 4, means ± SEM, one-way ANOVA multiple comparisons test with Sidak´s correction, * $p \leq 0.05$, ** $p \leq 0.01$). Figure kindly provided by Dr. Eleni Petsouki.

Analyzing the qPCR results, it should first be noted that previous experiments using KEAP1-/- MEF cells (data not shown) as well as investigations with NRF2-/- MEF cells conducted by Matzinger et al. 2020 have shown that without overexpressing β-TrCP2 the AMPK-dependent phospho-sites have no detectable effect on the gene expression of *Gclc* [7].

However, in the context of co-transfection with β-TrCP2 in a KEAP1 knockout background, as performed within the scope of this thesis, cells expressing the wild type and those expressing the mutant version of NRF2 exhibit a significantly different *Gclc* gene expression. Here, cells transfected with mutant NRF2 show increased *Gclc* mRNA levels compared to the wild type presumably because TM-NRF2 interacts less with the co-transfected β-TrCP2, is therefore more stable than WT-NRF2 and more available for initiating target gene transcription. Hence, the difference in *Gclc* expression levels between cells expressing WT- and TM-NRF2 reflects the abundance of NRF2 available for initiating gene expression in each setting. Thus, the results of the NRF2 gene expression experiments confirm the established hypothesis that the AMPK-dependent phosphorylation sites in NRF2 mediate its degradation via β-TrCP2.

Concerning the lack of significant qPCR results with the 4 h experiments (data not shown), it seems safe to assume that at this timepoint the induced overexpression of the transcription factor has not yet had any implications for the cells´ gene expression.

The increase in *Gclc* expression upon AMPK activation occurs irrespective of the transfected version of NRF2 and can be attributed to the AMPK-dependent phosphorylation of Ser558, which Joo et al. 2016 proved to induce nuclear accumulation of NRF2 [93]. Accordingly, the nuclear accumulation affects WT- and TM-NRF2 equally and thus explains why in both cases the *Gclc* expression levels rise upon exposure to the AMPK activator. These results also reinforce the model proposed on the nuclear increase of PLA signals upon AMPK activation (Ch. 3.2, Fig. 13B): The AMPK-mediated rise in *Gclc* expression regardless of the transfected NRF2 version proves that the AMPK-dependent nuclear accumulation of NRF2 forms occurs independently of the mutation. Besides that, AMPK may also generally impact NRF2 target gene expression via other pathways e.g., epigenetically [10].

4 Conclusions

The aim of this master thesis was to investigate the influence of three AMPK-dependent phosphorylation sites on the regulation of NRF2 through β-TrCP2. In doing so, the β-TrCP2-mediated regulation of NRF2 was examined under KEAP1 depleted conditions.

The findings of this thesis demonstrate that the mutation of the AMPK-dependent phospho-sites impedes interaction between NRF2 and β-TrCP2 resulting in higher NRF2 protein stability and consequently higher expression of certain NRF2 target genes like *Gclc*. It can thus be concluded that the AMPK-dependent phosphorylation of NRF2 at Ser374, Ser408 and Ser433 increases interactions between NRF2 and β-TrCP2 which enhances NRF2 degradation and negatively affects NRF2 target gene expression.

Accordingly, the results gathered during this thesis reveal AMPK to exert a downregulating effect on NRF2 under certain conditions. This outcome is remarkable as previous studies on the crosstalk between AMPK and NRF2 have so far shown AMPK activation to generally bring about an increase in NRF2 activity. However, the detected results could only be obtained under very specific experimental settings – that is with KEAP1 knockout.

Nevertheless, the current findings are an important contribution towards a better understanding of NRF2 regulation independently of KEAP1 and help gaining mechanistic insight into the direct crosstalk between AMPK and NRF2. Moreover, they also are a step towards comprehending the role of AMPK in a pathological setting such as cancer cells with KEAP1 mutations that lead to NRF2 hyperactivation. In this respect, further elucidation of the effect of AMPK activation on the degradation of overactive NRF2 may prompt new therapeutic approaches for treating such cancer types.

5 References

[1] V. Ngo, M.L. Duennwald, Nrf2 and Oxidative Stress: A General Overview of Mechanisms and Implications in Human Disease, Antioxidants. 11 (2022) 2345. https://doi.org/10.3390/antiox11122345.

[2] S. Menegon, A. Columbano, S. Giordano, The Dual Roles of NRF2 in Cancer, Trends in Molecular Medicine. 22 (2016) 578–593. https://doi.org/10.1016/j.molmed.2016.05.002.

[3] M. Poornashree, H. Kumar, R. Ajmeer, R. Jain, V. Jain, Dual role of Nrf2 in cancer: molecular mechanisms, cellular functions and therapeutic interventions, Mol Biol Rep. 50 (2023) 1871–1883. https://doi.org/10.1007/s11033-022-08126-1.

[4] N. Camiña, T.M. Penning, Genetic and epigenetic regulation of the NRF2-KEAP1 pathway in human lung cancer, Br J Cancer. 126 (2022) 1244–1252. https://doi.org/10.1038/s41416-021-01642-0.

[5] W.C.M. Dempke, M. Reck, KEAP1/NRF2 (NFE2L2) mutations in NSCLC – Fuel for a superresistant phenotype?, Lung Cancer. 159 (2021) 10–17. https://doi.org/10.1016/j.lungcan.2021.07.006.

[6] M. Sánchez-Ortega, A.C. Carrera, A. Garrido, Role of NRF2 in Lung Cancer, Cells. 10 (2021) 1879. https://doi.org/10.3390/cells10081879.

[7] M. Matzinger, K. Fischhuber, D. Pölöske, K. Mechtler, E.H. Heiss, AMPK leads to phosphorylation of the transcription factor Nrf2, tuning transactivation of selected target genes, Redox Biology. 29 (2020) 101393. https://doi.org/10.1016/j.redox.2019.101393.

[8] K. Fischhuber, M. Matzinger, E.H. Heiss, AMPK Enhances Transcription of Selected Nrf2 Target Genes via Negative Regulation of Bach1, Front. Cell Dev. Biol. 8 (2020) 628. https://doi.org/10.3389/fcell.2020.00628.

[9] K. Zimmermann, J. Baldinger, B. Mayerhofer, A.G. Atanasov, V.M. Dirsch, E.H. Heiss, Activated AMPK boosts the Nrf2/HO-1 signaling axis—A role for the unfolded protein response, Free Radical Biology and Medicine. 88 (2015) 417–426. https://doi.org/10.1016/j.freeradbiomed.2015.03.030.

[10] E. Petsouki, S.N.S. Cabrera, E.H. Heiss, AMPK and NRF2: Interactive players in the same team for cellular homeostasis?, Free Radical Biology and Medicine. 190 (2022) 75–93. https://doi.org/10.1016/j.freeradbiomed.2022.07.014.

[11] J.D. Hayes, A.T. Dinkova-Kostova, The Nrf2 regulatory network provides an interface between redox and intermediary metabolism, Trends in Biochemical Sciences. 39 (2014) 199–218. https://doi.org/10.1016/j.tibs.2014.02.002.

[12] D. Malhotra, E. Portales-Casamar, A. Singh, S. Srivastava, D. Arenillas, C. Happel, C. Shyr, N. Wakabayashi, T.W. Kensler, W.W. Wasserman, S. Biswal, Global mapping of binding sites for Nrf2 identifies novel targets in cell survival response through ChIP-Seq profiling and

network analysis, Nucleic Acids Research. 38 (2010) 5718–5734. https://doi.org/10.1093/nar/gkq212.

[13] B.N. Chorley, M.R. Campbell, X. Wang, M. Karaca, D. Sambandan, F. Bangura, P. Xue, J. Pi, S.R. Kleeberger, D.A. Bell, Identification of novel NRF2-regulated genes by ChIP-Seq: influence on retinoid X receptor alpha, Nucleic Acids Research. 40 (2012) 7416–7429. https://doi.org/10.1093/nar/gks409.

[14] A. Cuadrado, G. Manda, A. Hassan, M.J. Alcaraz, C. Barbas, A. Daiber, P. Ghezzi, R. León, M.G. López, B. Oliva, M. Pajares, A.I. Rojo, N. Robledinos-Antón, A.M. Valverde, E. Guney, H.H.H.W. Schmidt, Transcription Factor NRF2 as a Therapeutic Target for Chronic Diseases: A Systems Medicine Approach, Pharmacol Rev. 70 (2018) 348–383. https://doi.org/10.1124/pr.117.014753.

[15] J. Alam, D. Stewart, C. Touchard, S. Boinapally, A.M.K. Choi, J.L. Cook, Nrf2, a Cap'n'Collar Transcription Factor, Regulates Induction of the Heme Oxygenase-1 Gene, Journal of Biological Chemistry. 274 (1999) 26071–26078. https://doi.org/10.1074/jbc.274.37.26071.

[16] A.K. Jaiswal, Regulation of genes encoding NAD(P)H:quinone oxidoreductases, Free Radical Biology and Medicine. 29 (2000) 254–262. https://doi.org/10.1016/S0891-5849(00)00306-3.

[17] A.C. Wild, H.R. Moinova, R.T. Mulcahy, Regulation of γ-Glutamylcysteine Synthetase Subunit Gene Expression by the Transcription Factor Nrf2, Journal of Biological Chemistry. 274 (1999) 33627–33636. https://doi.org/10.1074/jbc.274.47.33627.

[18] J.H. Matthews, X. Liang, V.J. Paul, H. Luesch, A Complementary Chemical and Genomic Screening Approach for Druggable Targets in the Nrf2 Pathway and Small Molecule Inhibitors to Overcome Cancer Cell Drug Resistance, ACS Chem. Biol. 13 (2018) 1189–1199. https://doi.org/10.1021/acschembio.7b01025.

[19] P. Moi, K. Chan, I. Asunis, A. Cao, Y.W. Kan, Isolation of NF-E2-related factor 2 (Nrf2), a NF-E2-like basic leucine zipper transcriptional activator that binds to the tandem NF-E2/AP1 repeat of the beta-globin locus control region., Proc. Natl. Acad. Sci. U.S.A. 91 (1994) 9926–9930. https://doi.org/10.1073/pnas.91.21.9926.

[20] A. Kopacz, A.I. Rojo, C. Patibandla, D. Lastra-Martínez, A. Piechota-Polanczyk, D. Kloska, A. Jozkowicz, C. Sutherland, A. Cuadrado, A. Grochot-Przeczek, Overlooked and valuable facts to know in the NRF2/KEAP1 field, Free Radical Biology and Medicine. 192 (2022) 37–49. https://doi.org/10.1016/j.freeradbiomed.2022.08.044.

[21] K. Itoh, N. Wakabayashi, Y. Katoh, T. Ishii, K. Igarashi, J.D. Engel, M. Yamamoto, Keap1 represses nuclear activation of antioxidant responsive elements by Nrf2 through binding to the amino-terminal Neh2 domain, Genes Dev. 13 (1999) 76–86. https://doi.org/10.1101/gad.13.1.76.

[22] Y. Katoh, K. Itoh, E. Yoshida, M. Miyagishi, A. Fukamizu, M. Yamamoto, Two domains of Nrf2 cooperatively bind CBP, a CREB binding protein, and synergistically activate transcription: Synergistic activation of Nrf2 by CBP, Genes to Cells. 6 (2001) 857–868. https://doi.org/10.1046/j.1365-2443.2001.00469.x.

[23] P. Nioi, T. Nguyen, P.J. Sherratt, C.B. Pickett, The Carboxy-Terminal Neh3 Domain of Nrf2 Is Required for Transcriptional Activation, Mol Cell Biol. 25 (2005) 10895–10906. https://doi.org/10.1128/MCB.25.24.10895-10906.2005.

[24] P. Rada, A.I. Rojo, S. Chowdhry, M. McMahon, J.D. Hayes, A. Cuadrado, SCF/β-TrCP Promotes Glycogen Synthase Kinase 3-Dependent Degradation of the Nrf2 Transcription Factor in a Keap1-Independent Manner, Mol Cell Biol. 31 (2011) 1121–1133. https://doi.org/10.1128/MCB.01204-10.

[25] H. Wang, K. Liu, M. Geng, P. Gao, X. Wu, Y. Hai, Y. Li, Y. Li, L. Luo, J.D. Hayes, X.J. Wang, X. Tang, RXRα Inhibits the NRF2-ARE Signaling Pathway through a Direct Interaction with the Neh7 Domain of NRF2, Cancer Research. 73 (2013) 3097–3108. https://doi.org/10.1158/0008-5472.CAN-12-3386.

[26] L. Baird, M. Yamamoto, The Molecular Mechanisms Regulating the KEAP1-NRF2 Pathway, Mol Cell Biol. 40 (2020) e00099-20. https://doi.org/10.1128/MCB.00099-20.

[27] K. Itoh, N. Wakabayashi, Y. Katoh, T. Ishii, T. O'Connor, M. Yamamoto, Keap1 regulates both cytoplasmic-nuclear shuttling and degradation of Nrf2 in response to electrophiles: Keap1 regulation of Nrf2 degradation, Genes to Cells. 8 (2003) 379–391. https://doi.org/10.1046/j.1365-2443.2003.00640.x.

[28] A.V. Ulasov, A.A. Rosenkranz, G.P. Georgiev, A.S. Sobolev, Nrf2/Keap1/ARE signaling: Towards specific regulation, Life Sciences. 291 (2022) 120111. https://doi.org/10.1016/j.lfs.2021.120111.

[29] H. Motohashi, F. Katsuoka, J.D. Engel, M. Yamamoto, Small Maf proteins serve as transcriptional cofactors for keratinocyte differentiation in the Keap1–Nrf2 regulatory pathway, Proc. Natl. Acad. Sci. U.S.A. 101 (2004) 6379–6384. https://doi.org/10.1073/pnas.0305902101.

[30] H. Sekine, K. Okazaki, N. Ota, H. Shima, Y. Katoh, N. Suzuki, K. Igarashi, M. Ito, H. Motohashi, M. Yamamoto, The Mediator Subunit MED16 Transduces NRF2-Activating Signals into Antioxidant Gene Expression, Mol Cell Biol. 36 (2016) 407–420. https://doi.org/10.1128/MCB.00785-15.

[31] C. Tonelli, I.I.C. Chio, D.A. Tuveson, Transcriptional Regulation by Nrf2, Antioxidants & Redox Signaling. 29 (2018) 1727–1745. https://doi.org/10.1089/ars.2017.7342.

[32] J.D. Hayes, S. Chowdhry, A.T. Dinkova-Kostova, C. Sutherland, Dual regulation of transcription factor Nrf2 by Keap1 and by the combined actions of β-TrCP and GSK-3, Biochemical Society Transactions. 43 (2015) 611–620. https://doi.org/10.1042/BST20150011.

[33] A. Kobayashi, M.-I. Kang, H. Okawa, M. Ohtsuji, Y. Zenke, T. Chiba, K. Igarashi, M. Yamamoto, Oxidative Stress Sensor Keap1 Functions as an Adaptor for Cul3-Based E3 Ligase To Regulate Proteasomal Degradation of Nrf2, Mol Cell Biol. 24 (2004) 7130–7139. https://doi.org/10.1128/MCB.24.16.7130-7139.2004.

[34] M. McMahon, N. Thomas, K. Itoh, M. Yamamoto, J.D. Hayes, Dimerization of Substrate Adaptors Can Facilitate Cullin-mediated Ubiquitylation of Proteins by a "Tethering" Mechanism, Journal of Biological Chemistry. 281 (2006) 24756–24768. https://doi.org/10.1074/jbc.M601119200.

[35] A.-L. Levonen, A. Landar, A. Ramachandran, E.K. Ceaser, D.A. Dickinson, G. Zanoni, J.D. Morrow, V.M. Darley-Usmar, Cellular mechanisms of redox cell signalling: role of cysteine modification in controlling antioxidant defences in response to electrophilic lipid oxidation products, Biochemical Journal. 378 (2004) 373–382. https://doi.org/10.1042/bj20031049.

[36] P. Canning, F.J. Sorrell, A.N. Bullock, Structural basis of Keap1 interactions with Nrf2, Free Radical Biology and Medicine. 88 (2015) 101–107. https://doi.org/10.1016/j.freeradbiomed.2015.05.034.

[37] K.I. Tong, Y. Katoh, H. Kusunoki, K. Itoh, T. Tanaka, M. Yamamoto, Keap1 Recruits Neh2 through Binding to ETGE and DLG Motifs: Characterization of the Two-Site Molecular Recognition Model, Mol Cell Biol. 26 (2006) 2887–2900. https://doi.org/10.1128/MCB.26.8.2887-2900.2006.

[38] T. Fukutomi, K. Takagi, T. Mizushima, N. Ohuchi, M. Yamamoto, Kinetic, Thermodynamic, and Structural Characterizations of the Association between Nrf2-DLGex Degron and Keap1, Mol Cell Biol. 34 (2014) 832–846. https://doi.org/10.1128/MCB.01191-13.

[39] P. Canning, C.D.O. Cooper, T. Krojer, J.W. Murray, A.C.W. Pike, A. Chaikuad, T. Keates, C. Thangaratnarajah, V. Hojzan, B.D. Marsden, O. Gileadi, S. Knapp, F. von Delft, A.N. Bullock, Structural Basis for Cul3 Protein Assembly with the BTB-Kelch Family of E3 Ubiquitin Ligases, Journal of Biological Chemistry. 288 (2013) 7803–7814. https://doi.org/10.1074/jbc.M112.437996.

[40] L. Buetow, D.T. Huang, Structural insights into the catalysis and regulation of E3 ubiquitin ligases, Nat Rev Mol Cell Biol. 17 (2016) 626–642. https://doi.org/10.1038/nrm.2016.91.

[41] S. Tao, P. Liu, G. Luo, M. Rojo de la Vega, H. Chen, T. Wu, J. Tillotson, E. Chapman, D.D. Zhang, p97 Negatively Regulates NRF2 by Extracting Ubiquitylated NRF2 from the KEAP1-CUL3 E3 Complex, Mol Cell Biol. 37 (2017) e00660-16. https://doi.org/10.1128/MCB.00660-16.

[42] K.I. Tong, B. Padmanabhan, A. Kobayashi, C. Shang, Y. Hirotsu, S. Yokoyama, M. Yamamoto, Different Electrostatic Potentials Define ETGE and DLG Motifs as Hinge and Latch in Oxidative Stress Response, Mol Cell Biol. 27 (2007) 7511–7521. https://doi.org/10.1128/MCB.00753-07.

[43] Y. Horie, T. Suzuki, J. Inoue, T. Iso, G. Wells, T.W. Moore, T. Mizushima, A.T. Dinkova-Kostova, T. Kasai, T. Kamei, S. Koshiba, M. Yamamoto, Molecular basis for the disruption of Keap1–Nrf2 interaction via Hinge & Latch mechanism, Commun Biol. 4 (2021) 576. https://doi.org/10.1038/s42003-021-02100-6.

[44] J. Jin, T. Cardozo, R.C. Lovering, S.J. Elledge, M. Pagano, J.W. Harper, Systematic analysis and nomenclature of mammalian F-box proteins, Genes Dev. 18 (2004) 2573–2580. https://doi.org/10.1101/gad.1255304.

[45] D. Cui, X. Dai, J. Shu, Y. Ma, D. Wei, X. Xiong, Y. Zhao, The cross talk of two family members of β-TrCP in the regulation of cell autophagy and growth, Cell Death Differ. 27 (2020) 1119–1133. https://doi.org/10.1038/s41418-019-0402-x.

[46] Y. Bi, D. Cui, X. Xiong, Y. Zhao, The characteristics and roles of β-TrCP1/2 in carcinogenesis, FEBS J. 288 (2021) 3351–3374. https://doi.org/10.1111/febs.15585.

[47] S. Chowdhry, Y. Zhang, M. McMahon, C. Sutherland, A. Cuadrado, J.D. Hayes, Nrf2 is controlled by two distinct β-TrCP recognition motifs in its Neh6 domain, one of which can be modulated by GSK-3 activity, Oncogene. 32 (2013) 3765–3781. https://doi.org/10.1038/onc.2012.388.

[48] P. Rada, A.I. Rojo, N. Evrard-Todeschi, N.G. Innamorato, A. Cotte, T. Jaworski, J.C. Tobón-Velasco, H. Devijver, M.F. García-Mayoral, F. Van Leuven, J.D. Hayes, G. Bertho, A. Cuadrado, Structural and Functional Characterization of Nrf2 Degradation by the Glycogen Synthase Kinase 3/β-TrCP Axis, Mol Cell Biol. 32 (2012) 3486–3499. https://doi.org/10.1128/MCB.00180-12.

[49] A. Cuadrado, Structural and functional characterization of Nrf2 degradation by glycogen synthase kinase 3/β-TrCP, Free Radical Biology and Medicine. 88 (2015) 147–157. https://doi.org/10.1016/j.freeradbiomed.2015.04.029.

[50] Y. Watai, A. Kobayashi, H. Nagase, M. Mizukami, J. McEvoy, J.D. Singer, K. Itoh, M. Yamamoto, Subcellular localization and cytoplasmic complex status of endogenous Keap1, Genes Cells. 12 (2007) 1163–1178. https://doi.org/10.1111/j.1365-2443.2007.01118.x.

[51] J. Putters, J.A. Slotman, J.P. Gerlach, G.J. Strous, Specificity, location and function of βTrCP isoforms and their splice variants, Cellular Signalling. 23 (2011) 641–647. https://doi.org/10.1016/j.cellsig.2010.11.015.

[52] A. Kuga, K. Tsuchida, H. Panda, M. Horiuchi, A. Otsuki, K. Taguchi, F. Katsuoka, M. Suzuki, M. Yamamoto, The β-TrCP-Mediated Pathway Cooperates with the Keap1-Mediated Pathway in Nrf2 Degradation *In Vivo*, Mol Cell Biol. 42 (2022) e00563-21. https://doi.org/10.1128/mcb.00563-21.

[53] D.G. Hardie, F.A. Ross, S.A. Hawley, AMPK: a nutrient and energy sensor that maintains energy homeostasis, Nat Rev Mol Cell Biol. 13 (2012) 251–262. https://doi.org/10.1038/nrm3311.

[54] D.G. Hardie, B.E. Schaffer, A. Brunet, AMPK: An Energy-Sensing Pathway with Multiple Inputs and Outputs, Trends in Cell Biology. 26 (2016) 190–201. https://doi.org/10.1016/j.tcb.2015.10.013.

[55] D. Garcia, R.J. Shaw, AMPK: Mechanisms of Cellular Energy Sensing and Restoration of Metabolic Balance, Molecular Cell. 66 (2017) 789–800. https://doi.org/10.1016/j.molcel.2017.05.032.

[56] S.-C. Lin, D.G. Hardie, AMPK: Sensing Glucose as well as Cellular Energy Status, Cell Metabolism. 27 (2018) 299–313. https://doi.org/10.1016/j.cmet.2017.10.009.

[57] E.C. Hinchy, A.V. Gruszczyk, R. Willows, N. Navaratnam, A.R. Hall, G. Bates, T.P. Bright, T. Krieg, D. Carling, M.P. Murphy, Mitochondria-derived ROS activate AMP-activated protein kinase (AMPK) indirectly, Journal of Biological Chemistry. 293 (2018) 17208–17217. https://doi.org/10.1074/jbc.RA118.002579.

[58] T. Jansen, M. Kvandová, A. Daiber, P. Stamm, K. Frenis, E. Schulz, T. Münzel, S. Kröller-Schön, The AMP-Activated Protein Kinase Plays a Role in Antioxidant Defense and Regulation of Vascular Inflammation, Antioxidants. 9 (2020) 525. https://doi.org/10.3390/antiox9060525.

[59] F.A. Ross, C. MacKintosh, D.G. Hardie, AMP-activated protein kinase: a cellular energy sensor that comes in 12 flavours, FEBS J. 283 (2016) 2987–3001. https://doi.org/10.1111/febs.13698.

[60] Y. Yan, X. Zhou, H. Xu, K. Melcher, Structure and Physiological Regulation of AMPK, IJMS. 19 (2018) 3534. https://doi.org/10.3390/ijms19113534.

[61] B. Xiao, M.J. Sanders, D. Carmena, N.J. Bright, L.F. Haire, E. Underwood, B.R. Patel, R.B. Heath, P.A. Walker, S. Hallen, F. Giordanetto, S.R. Martin, D. Carling, S.J. Gamblin, Structural basis of AMPK regulation by small molecule activators, Nat Commun. 4 (2013) 3017. https://doi.org/10.1038/ncomms4017.

[62] A. Woods, S.R. Johnstone, K. Dickerson, F.C. Leiper, L.G.D. Fryer, D. Neumann, U. Schlattner, T. Wallimann, M. Carlson, D. Carling, LKB1 Is the Upstream Kinase in the AMP-Activated Protein Kinase Cascade, Current Biology. 13 (2003) 2004–2008. https://doi.org/10.1016/j.cub.2003.10.031.

[63] S.A. Hawley, D.A. Pan, K.J. Mustard, L. Ross, J. Bain, A.M. Edelman, B.G. Frenguelli, D.G. Hardie, Calmodulin-dependent protein kinase kinase-β is an alternative upstream kinase for AMP-activated protein kinase, Cell Metabolism. 2 (2005) 9–19. https://doi.org/10.1016/j.cmet.2005.05.009.

[64] X. Gu, Y. Yan, S.J. Novick, A. Kovach, D. Goswami, J. Ke, M.H.E. Tan, L. Wang, X. Li, P.W. de Waal, M.R. Webb, P.R. Griffin, H.E. Xu, K. Melcher, Deconvoluting AMP-activated protein kinase (AMPK) adenine nucleotide binding and sensing, Journal of Biological Chemistry. 292 (2017) 12653–12666. https://doi.org/10.1074/jbc.M117.793018.

[65] F.-J. Xin, J. Wang, R.-Q. Zhao, Z.-X. Wang, J.-W. Wu, Coordinated regulation of AMPK activity by multiple elements in the α-subunit, Cell Res. 23 (2013) 1237–1240. https://doi.org/10.1038/cr.2013.121.

[66] B. Xiao, M.J. Sanders, E. Underwood, R. Heath, F.V. Mayer, D. Carmena, C. Jing, P.A. Walker, J.F. Eccleston, L.F. Haire, P. Saiu, S.A. Howell, R. Aasland, S.R. Martin, D. Carling, S.J. Gamblin, Structure of mammalian AMPK and its regulation by ADP, Nature. 472 (2011) 230–233. https://doi.org/10.1038/nature09932.

[67] G.R. Steinberg, D.G. Hardie, New insights into activation and function of the AMPK, Nat Rev Mol Cell Biol. 24 (2023) 255–272. https://doi.org/10.1038/s41580-022-00547-x.

[68] M.J. Sanders, Z.S. Ali, B.D. Hegarty, R. Heath, M.A. Snowden, D. Carling, Defining the Mechanism of Activation of AMP-activated Protein Kinase by the Small Molecule A-769662, a Member of the Thienopyridone Family, Journal of Biological Chemistry. 282 (2007) 32539–32548. https://doi.org/10.1074/jbc.M706543200.

[69] J.W. Scott, N. Ling, S.M.A. Issa, T.A. Dite, M.T. O'Brien, Z.-P. Chen, S. Galic, C.G. Langendorf, G.R. Steinberg, B.E. Kemp, J.S. Oakhill, Small Molecule Drug A-769662 and AMP Synergistically Activate Naive AMPK Independent of Upstream Kinase Signaling, Chemistry & Biology. 21 (2014) 619–627. https://doi.org/10.1016/j.chembiol.2014.03.006.

[70] R. Willows, M.J. Sanders, B. Xiao, B.R. Patel, S.R. Martin, J. Read, J.R. Wilson, J. Hubbard, S.J. Gamblin, D. Carling, Phosphorylation of AMPK by upstream kinases is required for activity in mammalian cells, Biochemical Journal. 474 (2017) 3059–3073. https://doi.org/10.1042/BCJ20170458.

[71] C. de Wendt, L. Espelage, S. Eickelschulte, C. Springer, L. Toska, A. Scheel, A.D. Bedou, T. Benninghoff, S. Cames, T. Stermann, A. Chadt, H. Al-Hasani, Contraction-Mediated Glucose Transport in Skeletal Muscle Is Regulated by a Framework of AMPK, TBC1D1/4, and Rac1, Diabetes. 70 (2021) 2796–2809. https://doi.org/10.2337/db21-0587.

[72] Q. Wang, S. Liu, A. Zhai, B. Zhang, G. Tian, AMPK-Mediated Regulation of Lipid Metabolism by Phosphorylation, Biological & Pharmaceutical Bulletin. 41 (2018) 985–993. https://doi.org/10.1248/bpb.b17-00724.

[73] S. Wang, H. Li, M. Yuan, H. Fan, Z. Cai, Role of AMPK in autophagy, Front. Physiol. 13 (2022) 1015500. https://doi.org/10.3389/fphys.2022.1015500.

[74] Y. Chun, J. Kim, AMPK–mTOR Signaling and Cellular Adaptations in Hypoxia, IJMS. 22 (2021) 9765. https://doi.org/10.3390/ijms22189765.

[75] S. Herzig, R.J. Shaw, AMPK: guardian of metabolism and mitochondrial homeostasis, Nat Rev Mol Cell Biol. 19 (2018) 121–135. https://doi.org/10.1038/nrm.2017.95.

[76] A. Jain, T. Lamark, E. Sjøttem, K. Bowitz Larsen, J. Atesoh Awuh, A. Øvervatn, M. McMahon, J.D. Hayes, T. Johansen, p62/SQSTM1 Is a Target Gene for Transcription Factor NRF2 and Creates a Positive Feedback Loop by Inducing Antioxidant Response Element-

driven Gene Transcription, Journal of Biological Chemistry. 285 (2010) 22576–22591. https://doi.org/10.1074/jbc.M110.118976.

[77] I. Ryoo, M.-K. Kwak, Regulatory crosstalk between the oxidative stress-related transcription factor Nfe2l2/Nrf2 and mitochondria, Toxicology and Applied Pharmacology. 359 (2018) 24–33. https://doi.org/10.1016/j.taap.2018.09.014.

[78] G.A. Shilovsky, V.V. Ashapkin, Transcription Factor Nrf2 and Mitochondria – Friends or Foes in the Regulation of Aging Rate, Biochemistry Moscow. 87 (2022) 1477–1486. https://doi.org/10.1134/S0006297922120057.

[79] Y. Ren, H.-M. Shen, Critical role of AMPK in redox regulation under glucose starvation, Redox Biology. 25 (2019) 101154. https://doi.org/10.1016/j.redox.2019.101154.

[80] C. Mo, L. Wang, J. Zhang, S. Numazawa, H. Tang, X. Tang, X. Han, J. Li, M. Yang, Z. Wang, D. Wei, H. Xiao, The Crosstalk Between Nrf2 and AMPK Signal Pathways Is Important for the Anti-Inflammatory Effect of Berberine in LPS-Stimulated Macrophages and Endotoxin-Shocked Mice, Antioxidants & Redox Signaling. 20 (2014) 574–588. https://doi.org/10.1089/ars.2012.5116.

[81] X. Bai, Y. Zhu, J. Jie, D. Li, L. Song, J. Luo, Maackiain protects against sepsis via activating AMPK/Nrf2/HO-1 pathway, International Immunopharmacology. 108 (2022) 108710. https://doi.org/10.1016/j.intimp.2022.108710.

[82] Y.-L. Qiu, X.-N. Cheng, F. Bai, L.-Y. Fang, H.-Z. Hu, D.-Q. Sun, Aucubin protects against lipopolysaccharide-induced acute pulmonary injury through regulating Nrf2 and AMPK pathways, Biomedicine & Pharmacotherapy. 106 (2018) 192–199. https://doi.org/10.1016/j.biopha.2018.05.070.

[83] X. Xu, Q. Liu, J. Li, M. Xiao, T. Gao, X. Zhang, G. Lu, J. Wang, Y. Guo, P. Wen, J. Gu, Co-Treatment With Resveratrol and FGF1 Protects Against Acute Liver Toxicity After Doxorubicin Treatment via the AMPK/NRF2 Pathway, Front. Pharmacol. 13 (2022) 940406. https://doi.org/10.3389/fphar.2022.940406.

[84] Z.-M. Sun, P. Guan, L.-F. Luo, L.-Y. Qin, N. Wang, Y.-S. Zhao, E.-S. Ji, Resveratrol protects against CIH-induced myocardial injury by targeting Nrf2 and blocking NLRP3 inflammasome activation, Life Sciences. 245 (2020) 117362. https://doi.org/10.1016/j.lfs.2020.117362.

[85] X. Ci, J. Zhou, H. Lv, Q. Yu, L. Peng, S. Hua, Betulin exhibits anti-inflammatory activity in LPS-stimulated macrophages and endotoxin-shocked mice through an AMPK/AKT/Nrf2-dependent mechanism, Cell Death Dis. 8 (2017) e2798–e2798. https://doi.org/10.1038/cddis.2017.39.

[86] H. Lv, Q. Liu, Z. Wen, H. Feng, X. Deng, X. Ci, Xanthohumol ameliorates lipopolysaccharide (LPS)-induced acute lung injury via induction of AMPK/GSK3β-Nrf2 signal axis, Redox Biology. 12 (2017) 311–324. https://doi.org/10.1016/j.redox.2017.03.001.

[87] J. Duan, Y. Guan, F. Mu, C. Guo, E. Zhang, Y. Yin, G. Wei, Y. Zhu, J. Cui, J. Cao, Y. Weng, Y. Wang, M. Xi, A. Wen, Protective effect of butin against ischemia/reperfusion-induced myocardial injury in diabetic mice: involvement of the AMPK/GSK-3β/Nrf2 signaling pathway, Sci Rep. 7 (2017) 41491. https://doi.org/10.1038/srep41491.

[88] H. Lv, L. Hong, Y. Tian, C. Yin, C. Zhu, H. Feng, Corilagin alleviates acetaminophen-induced hepatotoxicity via enhancing the AMPK/GSK3β-Nrf2 signaling pathway, Cell Commun Signal. 17 (2019) 2. https://doi.org/10.1186/s12964-018-0314-2.

[89] X. Fan, L. Wang, J. Huang, H. Lv, X. Deng, X. Ci, Pterostilbene Reduces Acetaminophen-Induced Liver Injury by Activating the Nrf2 Antioxidative Defense System via the AMPK/Akt/GSK3β Pathway, Cell Physiol Biochem. 49 (2018) 1943–1958. https://doi.org/10.1159/000493655.

[90] Y. Sun, S. Zhou, H. Guo, J. Zhang, T. Ma, Y. Zheng, Z. Zhang, L. Cai, Protective effects of sulforaphane on type 2 diabetes-induced cardiomyopathy via AMPK-mediated activation of lipid metabolic pathways and NRF2 function, Metabolism. 102 (2020) 154002. https://doi.org/10.1016/j.metabol.2019.154002.

[91] D.H. Lee, J.S. Park, Y.S. Lee, S.H. Bae, PERK prevents hepatic lipotoxicity by activating the p62-ULK1 axis-mediated noncanonical KEAP1-Nrf2 pathway, Redox Biology. 50 (2022) 102235. https://doi.org/10.1016/j.redox.2022.102235.

[92] D.H. Lee, J.S. Park, Y.S. Lee, J. Han, D.-K. Lee, S.W. Kwon, D.H. Han, Y.-H. Lee, S.H. Bae, SQSTM1/p62 activates NFE2L2/NRF2 via ULK1-mediated autophagic KEAP1 degradation and protects mouse liver from lipotoxicity, Autophagy. 16 (2020) 1949–1973. https://doi.org/10.1080/15548627.2020.1712108.

[93] M.S. Joo, W.D. Kim, K.Y. Lee, J.H. Kim, J.H. Koo, S.G. Kim, AMPK Facilitates Nuclear Accumulation of Nrf2 by Phosphorylating at Serine 550, Mol Cell Biol. 36 (2016) 1931–1942. https://doi.org/10.1128/MCB.00118-16.

[94] D. Mafra, L. Alvarenga, L.F.M.F. Cardozo, M.B. Stockler-Pinto, L.S. Nakao, P. Stenvinkel, P.G. Shiels, Inhibiting BTB domain and CNC homolog 1 (Bach1) as an alternative to increase Nrf2 activation in chronic diseases, Biochimica et Biophysica Acta (BBA) - General Subjects. 1866 (2022) 130129. https://doi.org/10.1016/j.bbagen.2022.130129.

[95] A.K. Jain, A.K. Jaiswal, GSK-3β Acts Upstream of Fyn Kinase in Regulation of Nuclear Export and Degradation of NF-E2 Related Factor 2, Journal of Biological Chemistry. 282 (2007) 16502–16510. https://doi.org/10.1074/jbc.M611336200.

6 Appendix

6.1 List of abbreviations

A

ACC1 ..... *Acetyl-CoA carboxylase 1*

ACC2 ..... *Acetyl-CoA carboxylase 2*

ADaM ..... *Allosteric drug and metabolite-binding site*

ADP ..... *Adenosine diphosphate*

AICAR ..... *5-Aminoimidazole-4-carboxamide ribonucleoside*

α-AID ..... *Auto-inhibitory domain of the α-subunit*

alpha-PAL ..... *Alpha palindromic-binding protein*

AMP ..... *Adenosine monophosphate*

AMPK ..... *5´-AMP-activated protein kinase*

APS ..... *Ammonium persulfate*

ARE ..... *Antioxidant response element*

ATP ..... *Adenosine triphosphate*

B

BACH1 ..... *BTB domain and CNC homology 1 transcription regulator protein*

BSA ..... *Bovine serum albumine*

bZIP ..... *Basic region leucine zipper*

C

CAMKK2 ..... *Calcium/calmodulin-dependent protein kinase kinase 2*

β-CBM ..... *Carbohydrate binding module of the β-subunit*

CBP ..... *CREB-binding protein*

CBS1-4 ..... *Cystathione β-synthase motifs 1-4*

cDNA ..... *Complementary DNA*

CHD6 ..... *Chromodomain helicase DNA-binding protein 6*

CHX ..... *Cycloheximide*

C-lobe ..... *Carboxy-terminal lobe*

CNC ..... *Cap´n´collar*

Ct ..... *Cycle threshold*

α-CTD ..... *Carboxy-terminal domain of the α-subunit*

β-CTD ..... *Carboxy-terminal domain of the β-subunit*

CUL1 ..... *Cullin-1*

CUL3 ..... *Cullin-3*

D

DAPI ..... *4´,6-Diamidino-2-phenylindole*

DMEM ..... *Dulbecco´s Modified Eagle´s Medium*

DNA ..... *Deoxyribonucleic acid*

dNTP ..... *Deoxynucleoside triphosphate*

DTT ..... *Dithiothreitol*

DUSP4 ..... *Dual specificity phosphatase 4*

E

EDTA ..... *Ethylenediaminetetraacetic acid*

EGFP ..... *Enhanced green fluorescent protein*

F

FBS ..... *Fetal Bovine Serum*

FBXW ..... *F-box and WD repeat domain containing*

G

Gclc ..... *Glutamate-cysteine ligase catalytic subunit*

GLUT4 ..... *Glucose transporter type 4*

GSK-3 ..... *Glycogen synthase kinase-3*

H

HA ..... *Influenza haemagglutinin tag*

HEK ..... *Human embryonic kidney cells*

HMGCR ..... *3-Hydroxy-3-methyl-glutaryl-CoA reductase*

Hmox1 ..... *Heme oxygenase 1*

I

IVR ..... *Intervening region*

K

α-KD ..... *Kinase domain of the α subunit*

KEAP1 ..... *Kelch-like ECH-associated protein 1*

L

LAS X ..... *Leica Application Suite X*

LKB1 ..... *Liver kinase B1*

M

MEF ..... *Mouse embryonic fibroblasts*

mTORC1 ..... *Mechanistic target of rapamycin complex 1*

N

NADPH ..... *Nicotinamide adenine dinucleotide phosphate*

Neh1-7 ..... *Nrf2-ECH homology domain*

Nqo1 ..... *NAD(P)H quinone dehydrogenase 1*

NRF2 ..... *Nuclear factor erythroid 2-related factor 2*

NSCLC ..... *Non-small cell lung cancer*

P

PAA ..... *Polyacrylic acid*

PBS ..... *Phosphate buffered saline*

PGC1α ..... *Peroxisome proliferator-activated receptor gamma co-activator 1α*

PINK1 ..... *PTEN-induced kinase 1*

PLA ..... *Proximity Ligation Assay*

PMSF ..... *Phenylmethylsulfonyl fluoride*

PTEN ..... *Phosphatase and tensin homolog*

PVDF ..... *Polyvinylidene difluoride*

Q

qPCR ..... *Quantitative Polymerase Chain Reaction*

R

RBX1 ..... *RING box protein 1*

α-RIM2 ..... *Regulatory subunit-interacting motif 2 of the α-subunit*

RIPA ..... *Radioimmunoprecipitation Assay*

RNA ..... *Ribonucleic acid*

RNase ..... *Ribonuclease*

ROS ..... *Reactive oxygen species*

RPTOR ..... *Regulatory-associated protein of mTOR*

RT ..... *Reverse transcription*

RXRα ..... *Retinoid X receptor α*

S

SCF *SKP1-CUL1-F-box*

SDS-PAGE ..... *Sodium dodecyl sulfate-polyacrylamide gel electrophoresis*

siRNA ..... *Small interfering RNA*

SKP1 ..... *S-phase kinase associated protein 1*

sMAF ..... *Small musculoaponeurotic fibrosarcoma protein*

SQSTM1/ p62 ..... *Sequestome 1*

T

TBC1D1/4 ..... *TBC1 domain family member 1 and 4*

TBP ..... *TATA-box binding protein*

TBS-T ..... *Tris buffered saline Tween 20*

TEMED ..... *Tetramethylethylenediamine*

TFAM ..... *Mitochondrial transcription factor A*

TM-NRF2 ..... *Triple mutant-NRF2*

β-TrCP ..... *β-Transducing repeat-containing protein*

Tris ..... *Tris(hydroxymethyl)aminomethane*

TSC2 ..... *Tuberous sclerosis complex 2*

U

ULK1 ..... *Unc51-like autophagy activating kinase 1*

W

WT-NRF2 ..... *Wild type-NRF2*

6.2 List of figures

6.3 Acknowledgements

First of all, I want to express my deep gratitude to Prof. Dr. Elke Heiß for agreeing to supervise my thesis and always offering kind words of advice and encouragement throughout my time here. I would also like to thank Dr. Eleni Petsouki for her close supervision, patient guidance and overall support during every part of my thesis. She was always available if any questions came up, provided me with motivating feedback and altogether made my work here an exciting and great experience. Many thanks also go to Shara Sosa Cabrera, BSc MSc who never hesitated to give me valuable advice on how to plan and write a thesis. Furthermore, I would like to express my appreciation to everyone of the Division of Pharmacognosy for always taking the time to answer any questions I had and generally creating such a pleasant working atmosphere.

At this point, I also want to thank my family, especially my parents, for always being patient, supporting and encouraging with my studies. Finally, I would like to mention my best friend, whose emotional support I can always count on.